Correspondence to:
C. E. Morales,
camorale@udec.cl

The Influence of Diapycnal Nutrient Fluxes on Phytoplankton Size Distribution in an Area of Intense Mesoscale and Submesoscale Activity off Concepción, Chile

A. Corredor-Acosta[1,2], C. E. Morales[2,3] (iD), A. Rodríguez-Santana[4] (iD), V. Anabalón[2] (iD), L. P. Valencia[2,5] (iD), and S. Hormazabal[2,5]

[1]Programa de Postgrado en Oceanografía, Departamento de Oceanografía, Facultad de Ciencias Naturales y Oceanográficas, Universidad de Concepción, Concepción, Chile, [2]Instituto Milenio de Oceanografía, Universidad de Concepción, Concepción, Chile, [3]Departamento de Oceanografía, Facultad de Ciencias Naturales y Oceanográficas, Universidad de Concepción, Concepción, Chile, [4]Departamento de Física, Facultad de Ciencias del Mar, Universidad de las Palmas de Gran Canaria, Las Palmas de Gran Canaria, España, [5]Escuela de Ciencias del Mar, Facultad de Ciencias del Mar y Geografía, Pontificia Universidad Católica de Valparaíso, Valparaíso, Chile

Abstract Mesoscale and submesoscale processes that contribute to localized increases in nutrients in the sunlit layer can stimulate phytoplankton growth and community changes, but the mechanisms involved remain sparsely documented with in situ data in the case of Eastern Boundary Upwelling Systems (EBUSs) and of most ocean regions. The role of diapycnal mixing in providing nutrients to the upper layer and in influencing phytoplankton size structure was analyzed in an area of intense mesoscale and submesoscale activity during the coastal upwelling season off Concepción (~36–37°S), the Humboldt Current EBUS. Diapycnal nutrient fluxes based on conductivity, temperature, and depth vertical eddy diffusivity (K_z) values (the Thorpe scale method) and on nutrient gradients were assessed in association with size-fractionated chlorophyll-a and microdiatom abundance derived from in situ sampling in an area including a mesoscale intrathermocline eddy (ITE) adjacent to a coastal upwelling front (CUF). The indirect estimates of K_z values spanned between 0.01 and 4×10^{-4} m^2 s^{-1}, and maxima in diapycnal nitrate flux per station ranged between 0.08 and 19.1 mmol m^{-2} day^{-1}. Maxima in the upward fluxes were detected at the subsurface (15–40 m depth) in the CUF and ITE areas, coinciding with maxima in the micro- and nano-chlorophyll-a fractions and in microdiatom abundance. These results suggest that ITE and CUF features, as well as their interaction, can generate intense diapycnal mixing and, thereby, contribute to increasing nutrient availability below the mixed layer. In turn, these processes enhance the contribution of larger phytoplankton cells in the coastal transition zone of EBUSs.

Plain Language Summary Phytoplankton in the upper ocean are the main primary producers of organic matter based on light, inorganic carbon (CO_2), and nutrients. These cells range from small to large sizes in the micrometer scale (~1–100 μm diameter). In coastal upwelling regions, wind-driven events lead to a nutrient enrichment favoring increases of primary production in the coastal zone and to a dominance of large phytoplankton, which require higher nutrient levels than do smaller cells. In contrast, in the oceanic nutrient-poor zone, smaller phytoplankton are usually dominant. However, mesoscale and submesoscale activity (fronts, eddies, meanders, and filaments) in the zone between the coastal and oceanic waters, the coastal transition zone (CTZ), can generate localized injections of nutrients toward the surface and, thereby, contribute to an enhancement of productivity and to changes in the community in the CTZ. Several mechanisms can contribute to such injections, but field observations to document them are sparse. Based on observations in an area of intense mesoscale and submesoscale activity, we provide evidence of the contribution of the turbulent mixing in locally increasing nutrient availability in the upper layer and, in turn, to sustain patches of large-size phytoplankton cells in the CTZ.

1. Introduction

Mesoscale and submesoscale physical processes in the ocean have been identified as important contributors to the transport and mixing of tracers (e.g., nutrients, oxygen, and plankton) through diverse mechanisms, thereby influencing directly biological communities and biogeochemical cycles. However, observational

data of such processes and of their biological and biogeochemical effects remain sparse due to their transient nature, requiring higher spatiotemporal sampling resolution (~0.1 km to tens of kilometers) compared to those linked with larger scales of variability. At the same time, the mesoscale and submesoscale dimensions are strongly intermingled because of the energy transfers and transformations generated at these scales, besides those derived from larger and smaller scales, which leads to the coexistence of geostrophic and ageostrophic dynamics (see reviews in Klein & Lapeyre, 2009; Mahadevan, 2016; McGillicuddy, 2016; Klein et al., 2019). Mesoscale to submesoscale dynamics can lead to changes in nutrient availability and, thereby, in phytoplankton growth rates and community composition (see reviews in Lévy et al., 2018; Mahadevan, 2016; McGillicuddy, 2016). In Eastern Boundary Upwelling Systems (EBUSs), characterized by the regular occurrence of wind-driven upwelling of nutrient-rich waters in the coastal zone (CZ), intense mesoscale and submesoscale activity in the coastal transition zone (CTZ) is reflected in the formation of features such as eddies, filaments, jets, meanders, and fronts (Brink & Cowles, 1991; Capet et al., 2014; Chaigneau et al., 2009; Pegliasco et al., 2015). EBUS coastal upwelling leads to high levels of phytoplankton biomass and primary production; however, patches of moderate biomass levels are also detected in the CTZ and, in association with mesoscale and submesoscale dynamics, contribute to an offshore advection of waters nearest to the CZ and/or through local growth in the CTZ, mediated by vertical injections of nutrients to the photic layer (Callbeck et al., 2017; Chenillat et al., 2015; Correa-Ramirez et al., 2007; Pietri et al., 2013).

Though mesoscale and submesoscale dynamics have been recognized as an important component of the variability in phytoplankton size structure, observational evidence is still sparse and the mechanisms remain unclear (Lamont et al., 2018; Rodríguez et al., 2001; Sangrà et al., 2014; Waga et al., 2019). Phytoplankton size structure is a key component in the ocean energy flow pathways and in the efficiency of an ecosystem to export carbon into the deep ocean, given the strong relationships between cell size and nutrient uptake, metabolic rates, light absorption, and food web structure (reviews in Finkel et al., 2010; Marañón, 2015; Mouw et al., 2016; Richardson, 2019). On this basis, its modulation by mesoscale and submesoscale physical-biological processes is highly relevant to understand the dynamics of marine ecosystems. In the case of a mesoscale cyclonic eddy in the subtropical North Pacific, submesoscale variability in phytoplankton size distribution was denoted by a dominance of large cells in the eddy center, where an intense vertical pulse of nutrients was detected. In addition, a dominance of smaller cells was detected in its edges, associated with an advective flux by isopycnal mixing and a continuous low nutrient supply (Brown et al., 2008). In the case of fronts, there is evidence in the California Current (CC) EBUS that increased diapycnal nitrate flux below the mixed layer takes place in a CTZ front. Based on modeling, it was concluded that an enhancement in the biomass of large phytoplankton at the front could be stimulated by this process, together with biological dynamics. This contradicts the traditional view that coastal phytoplankton accumulates at the front as a result of other physical processes (Li et al., 2012). A shift of phytoplankton size structure toward larger cells was also documented for the same front (Taylor et al., 2012).

In the EBUS off western South America, the Humboldt Current System (HCS), mesoscale surface and intrathermocline eddies (ITEs) generated near the coast are regularly detected (Chaigneau et al., 2011; Czeschel et al., 2018; Johnson & McTaggart, 2010). ITEs in the HCS transport Equatorial Subsurface Water (ESSW) associated with the poleward Peru-Chile Undercurrent (PCUC), which flows at the edge of the shelf and upper slope (Hormazabal et al., 2013; Thomsen et al., 2016). The ESSW, upwelling water mass, is characterized by higher salinity, minima in oxygen, and higher nutrient content, compared to surface waters in the region, such as the Subantartic Water (SAAW) and the Subtropical Water (SSTW) (Llanillo et al., 2012; Silva et al., 2009; Strub et al., 1998). The formation of these ITEs has been associated with instabilities in the PCUC derived from its interaction with the shelf-slope topography. This leads to anticyclonic vorticity and to conditions favorable for centrifugal instabilities, which in turn generate coherent submesoscale anticyclonic PCUC eddies. The latter coalesce as they travel offshore to generate mesoscale PCUC ITEs (Contreras et al., 2019; Thomsen et al., 2016). Centrifugal instabilities (i.e., inertial instabilities that extract energy from the mean current through horizontal shear) involve isopycnal and diapycnal mixing processes and small-scale turbulence in EBUSs (Contreras et al., 2019; Dewar et al., 2015). In EBUSs, besides horizontal advection of nutrients from the CZ to the CTZ by mesoscale and submesoscale features, diapycnal mixing has been identified as an important mechanism of vertical mixing in the CTZ. This is especially so at

the continental margin, contributing to vertical injections of gases, solutes, and organic matter toward the upper layer (Callbeck et al., 2017; Li et al., 2012; Loginova et al., 2019; Steinfeldt et al., 2015). The effects of diapycnal mixing on phytoplankton community size distribution in EBUSs based on observational data remain to be investigated.

In the HCS region off central southern Chile (33–40°S), where wind-driven coastal upwelling is seasonal, an intensified coastal upwelling front (CUF) has been reported during the summer (Letelier et al., 2009). Off Concepción (~36–37°S), the CUF is usually flanked by an ITE on the offshore side (Letelier et al., 2009; Morales et al., 2012). As for the effects of these features on phytoplankton, the stronger density gradients in the CUF off Concepción can act as a barrier to cross-shelf exchanges of phytoplankton, with a dominance of larger size cells on the coastal side and smaller ones in the oceanic side (Menschel et al., 2016; Morales et al., 2012). In the proximity of this CUF, 2-month old mesoscale eddies have been found to be dominated by picoplankton and nanoplankton cells, in contrast to the dominance of microplankton cells (mostly diatoms) in the CZ during the upwelling season (Morales et al., 2012). However, a dominance of the microplankton fraction during the early stages of eddy development closer to the coast and of smaller size fractions as eddies move offshore was found in the same area using a satellite approach of phytoplankton size classes (Corredor-Acosta et al., 2018). During an event of ITE-CUF interaction in the same area and in the early stages of ITE formation, increases of larger phytoplankton in the CUF and ITE areas and a cross-shelf exchange of diatom species from the CZ and CTZ were observed, together with intense submesoscale variability in macronutrient distribution (Morales et al., 2017). These results suggested that the ITE and CUF, as well as their interaction, probably lead to localized vertical injections of nutrients toward the upper layer, in addition to lateral advection of nutrient from coastal waters; however, the mechanisms contributing to such nutrient pathways have not been explored yet.

In this study, we explore the role of diapycnal mixing on locally providing nutrients to the upper layer and, thereby, fueling increases in phytoplankton biomass and producing a shift in the size structure in the CTZ off Concepción, based on data reported previously by Morales et al. (2017). The selection of this mechanism, diapycnal mixing, is based on background information available for EBUS regions and detailed above, which have identified it as an important contributor to localized vertical injection of solutes to the upper layer in the CTZ; this does not rule out the contribution of additional mechanisms, which could not be assessed during this study. For this purpose, the vertical eddy diffusivity (K_z) as an indicator of diapycnal turbulent mixing was estimated using indirect estimates through the Thorpe scale method. K_z and the vertical gradients in nutrient concentration were used to estimate diapycnal nutrient fluxes, while the distributions of chlorophyll-a (Chl-a) size fractions and microdiatom abundance were compared to those of diapycnal nutrient fluxes.

2. Materials and Methods

Satellite and in situ observational data obtained for this study in the area off Concepción (~36–37°S, 73–74.5°W; Figure 1) have been previously analyzed in terms of the oceanographic setting at the mesoscale and submesoscales dimensions, its relationship with the distribution of macronutrients, and phytoplankton composition and distribution in the upper water column (Morales et al., 2017). A summary of the methods employed is presented in sections 2.1 and 2.2, while the methods used in the present study are described in sections 2.3 and 2.4.

2.1. Satellite Surface Temperature, Geostrophic Circulation Field, and Chl-a

As background information for the field observations, the mean sea surface temperature (SST), mean surface geostrophic velocity field, and total Chl-a distributions were derived from satellite sources for the period of the in situ observations (PHYTO-FRONT cruise, 3-6 February 2014). SST was obtained from the daily Multi-scale Ultra-high Resolution Sea Surface Temperature (MUR-SST; https://podaac.jpl.nasa.gov/Multi-scale_Ultra-high_Resolution_MUR-SST) product with a spatial resolution of 1 km. The mean surface geostrophic velocity field was obtained from the Copernicus Marine and Environment Monitoring Service (CMEMS; http://marine.copernicus.eu/) product with a spatial resolution of 0.25° (~25 km). The mean surface total Chl-a was obtained from version 4.0 of the Ocean Colour Climate Change Initiative (OC-CCI, a
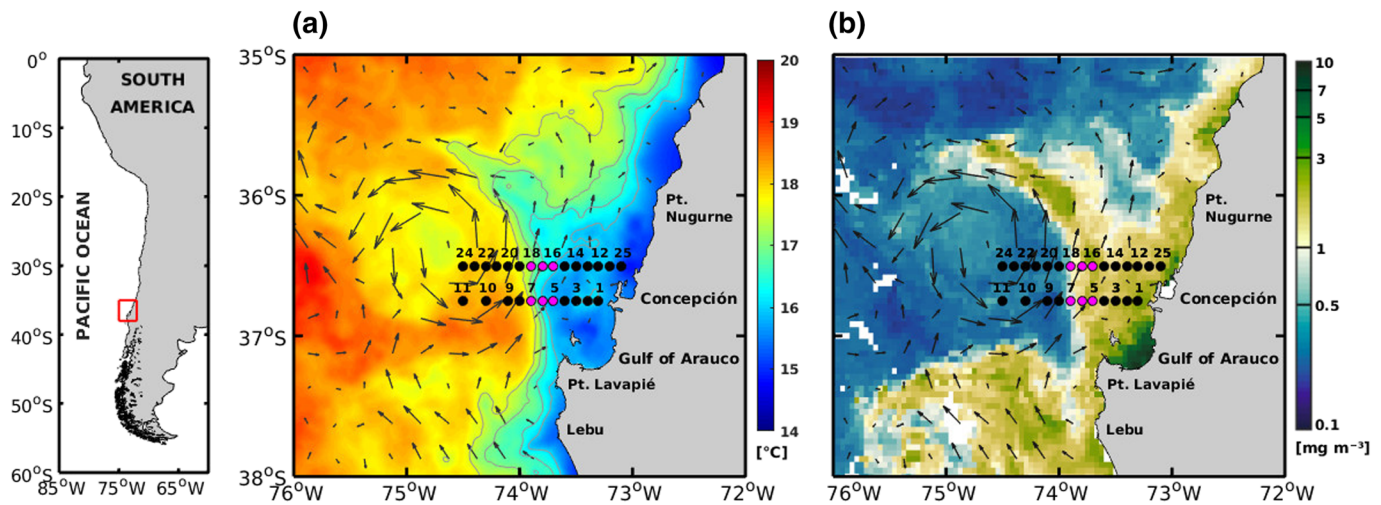
Figure 1. Map of South America indicating the study area (red rectangle) and satellite mean surface conditions during the PHYTO-FRONT cruise (3–7 February 2014). (a) Sea surface temperature (MUR-SST) and geostrophic circulation (CMEMS), and (b) total chlorophyll-a (Chl-a) concentration (ESA OC-CCI) and geostrophic circulation. Dots represent the position of the sampling stations in the northern (36.5°S, 73.1–74.5°W) and southern (36.75°S, 73.3–74.5°W) transects; magenta dots indicate the position of the coastal upwelling front (CUF; Stations 5–7 and 16–18). The gray lines in (a) indicate the isotherms of 16, 16.5, 17, and 17.5 °C from the coast to offshore, respectively.

merged product available at http://www.oceancolour.org/), at processing level 3 and a spatial resolution of 4 km.

2.2. In Situ Nutrients, Size-Fractionated Chl-a, and Microdiatom Abundance

Nutrient samples during the PHYTO-FRONT cruise were collected with Niskin bottles in the upper layer (0, 5, 10, 15, 20, 30, 40, 60, 80, and 100 m depth) and stored frozen (−20 °C) in aseptic high-density polyethylene flasks (60 ml) for subsequent analysis, following standard protocols (Atlas et al., 1971). Parallely, total and size-fractionated Chl-a samples in the microphytoplankton, nanophytoplankton, and picophytoplankton range were collected in the upper layer (0, 5, 10, 15, 20, 25, 30, 40, 60, 80, and 100 m depth) and filtered (~250 ml) using GF/F glass fiber filters (total), together with filters covering the size fractions (3 and 20 μm pore diameter). All measurements were taken in triplicate and frozen (−20 °C) until later analysis by fluorometry (Turner Design AU-10) following standard procedures (Anabalón et al., 2016). In addition, plankton samples were collected from the same bottles for composition and abundance analysis of the phytoplankton size fractions. In the case of diatoms, only the abundance in the microplankton size range is analyzed here.

2.3. Thorpe Scale, Vertical Eddy Diffusivity, and Diapycnal Nutrient Fluxes

Conductivity, temperature, and depth (CTD) casts (0–300 m depth) were performed during the PHYTO-FRONT cruise, using a Sea-Bird SBE 911plus CTD equipment that provides a 24 Hz sampling rate. To estimate the Thorpe scale, which is an energy-containing vertical overturning scale, the overturns generated by turbulence in the stratified part of the water column were detected through inversions in fine-scale vertical downcast density profiles. To do this using CTD data, a minimization of measurement errors and instrument noise is needed. To obtain a fine-scale density data, the following steps were taken, following the procedure described by Park et al. (2014). Based on the Sea-Bird processing software, two modules were applied. First, the "Cell Thermal Mass" module was performed to minimize the thermal lag arising from the conductivity cell thermal mass effects, using the recommended values ($\alpha = 0.03$, $1/\beta = 7.0$) for the SBE 911plus CTD. Second, the "Loop Edit" module was performed in order to avoid pressure reversals due to the effect of the ship while the CTD was falling down. A third one, the module "Align," was not executed since the CTD includes a deck unit that advances conductivity by 0.073 s regarding the temperature, removing automatically the salinity spiking caused by the misalignment between the two measurements.

Temperature and salinity downcast data were used to calculate potential density with the TEOS-10 subroutines for Matlab of the Gibbs-SeaWater (GSW) Oceanographic Toolbox (McDougall & Barker, 2011). The final vertical density profiles were subsampled at regular depth intervals of 10 cm. Each interval contained 2.4 scans, consistent with a mean fall speed of ~1 m s^{-1} and the 24 Hz CTD sampling rate. For all profiles, the first 10 to 20 m depth was removed from the analyses, to avoid surface turbulence generated by the ship and the mixed layer, since the Thorpe analysis is applicable only to the stable stratified part of the water column.

To calculate the overturns, the vertical density profile from each station was sorted to obtain a stable monotonic sequence. For this, a downward (top to bottom) intermediate density profile was obtained, maintaining a constant density until the density change was greater than a threshold value. Likewise, an upward (bottom to top) intermediate density profile was constructed. The final intermediate density profile for each station was represented by the average of the two (downward and upward) profiles (Gargett & Garner, 2008; Park et al., 2014). Therefore, differences in the intermediate density profile above a threshold level were considered as real overturns. In this study, the threshold noise value was 5×10^{-4} kg m^{-3}, calculated as the median of the density differences inside the "well-mixed" layer in all sampling profiles. Finally, the Thorpe scale (L_T) was estimated as the root-mean-square of an ensemble of vertical displacements (in meters) necessary to generate the stable vertical density profiles, computed at successive nonzero Thorpe displacements (Park et al., 2014; Sangrà et al., 2014).

Vertical eddy diffusivity coefficient (K_z) was then estimated using the Thorpe scale, following Ozmidov (1965) and Dillon (1982), which according to the Osborn parameterization (Osborn, 1980) is obtained as

$$K_z = 0.128 L_\mathrm{T}^2 N, \tag{1}$$

where N is the Brunt-Väisälä frequency or buoyancy frequency at which a fluid parcel oscillates when it is displaced from the stable state; it was calculated from the relation

$$N^2 = \frac{-g}{\rho_0} \frac{\partial \rho}{\partial z}, \tag{2}$$

where g is the gravitational acceleration, ρ_0 is the mean seawater density, and $\partial \rho / \partial z$ is the vertical density gradient. Maximum frequency values in the water column are expected where the stratification is strongest.

Diapycnal nutrient (nitrate, phosphate, and silicate or silicic acid) fluxes ($F_{Nutrient}$) were calculated through the relation

$$F_{Nutrient} = -K_z \frac{\partial Nutrient}{\partial z}, \tag{3}$$

where K_z is the vertical eddy diffusivity obtained in each sampling station and for the same depth range over which the vertical nutrient concentration gradient ($\partial Nutrient / \partial z$) was calculated (Girault et al., 2015). The K_z coefficient is an important measurement in the interpretation of turbulence dissipation rates and small-scale mixing processes. It is known by several names in the literature, including vertical diffusivity (Park et al., 2014), vertical turbulent diffusivity (Girault et al., 2015), diapycnal diffusivity (Ledwell et al., 2008; Li et al., 2012; Zhang et al., 2017), eddy diffusion coefficient (Lund-Hansen et al., 2006), eddy diffusivity (Rippeth et al., 2009) and vertical eddy diffusivity (Arcos-Pulido et al., 2014; Doubell et al., 2018; Henley et al., 2018; Hsu et al., 2019; Law et al., 2001). The appropriateness of K_z estimates based on CTD data depends on the relationship between the Thorpe and Ozmidov length scales. That is, a good agreement between these scales and a proper application of the Thorpe method will be obtained in flows where the turbulence is shear-driven and characterized by overturns in the order of tens of meters (Mater et al., 2015; Scotti, 2015).

2.4. Meridional Geostrophic Velocity and Mixed Layer Depth

Temperature and absolute salinity profiles obtained earlier were used to calculate potential density anomaly and meridional geostrophic velocity (Pond & Pickard, 2013). The geostrophic velocity (V_g) was computed every three stations along each transect and was obtained from the balance between planetary vorticity and the pressure gradient force as follows:

$$Vg = \frac{1}{f\rho_0}\frac{\partial P}{\partial x},$$

(4)

where f is the Coriolis parameter, ρ_0 is the mean seawater density, and $\partial P/\partial x$ is the pressure horizontal gradient from the geopotential anomaly relative to the sea surface. Additionally, the mixed layer depth was evaluated for each sampling station using a threshold value in density ($\Delta\rho = 0.03$ kg m^{-3}) from a near-surface depth of 10 m, following the procedure of de Boyer Montégut et al. (2004).

3. Results

3.1. General Oceanographic Setting

In situ sampling took place during a period of relaxation of upwelling-favorable winds, according to the description in Morales et al. (2017). Satellite data indicated that the sampling took place in a region of colder waters (<15 °C) in the CZ and warmer waters (>17 °C) in the CTZ, separated by a strong SST gradient denoted by the 16–17 °C isotherms (Stations 6–7 and 16–18, ~70–100 km from the coast) (Figure 1a). The geostrophic field indicated that adjacent to this thermal frontal, an anticyclonic mesoscale eddy (diameter of ~150 km) was located in the CTZ, such that offshore stations in the northern transect were distributed close to the eddy center and in its eastern edge, whereas in the southern transect, they were distributed on its southeastern edge (Figure 1a). Satellite surface total Chl-a values were highest (>3 mg m^{-3}) near the coast, and both moderate (~1–2 mg m^{-3}) and low values (<1 mg m^{-3}) were found in the CTZ (Figure 1b). An abrupt change from moderate to low surface Chl-a concentrations was observed westward from the front (Stations 7–8 and 18–19), together with an offshore plume of moderate values along a cold filament in the northern section of the eddy. Further, an onshore intrusion of low values associated with warm waters in the southern section of the same eddy was also observed (Figures 1a and 1b).

In upper water column (0–100 m depth), a strong uplift of isotherms and isohalines toward the coast was detected in both transects (Figures 2a, 2b, 2d, and 2e), with colder (<16°C) and higher-salinity (>34) waters reaching a shallower depth in the CZ than in CTZ waters, creating a CUF area (Stations 5–7 and 16–18). The CUF was characterized by a strong horizontal gradient in potential density (0.5–1 kg m^{-3} in 10 km) and also in the vertical dimension (Figures 2c and 2f). In the offshore area (Stations 10–11 and 21–24), a dome-shaped subsurface uplifting of the 25.7–26.2 isopycnals, together with an intrusion of high-salinity waters (>34.4; Figures 2b, 2c, 2e, and 2f), signaled the presence of an ITE. Between the CUF and the ITE, a pocket of waters with the lowest density and salinity was detected in both transects, more markedly in the southern transect (Figures 2b, 2c, 2e, and 2f). The strong steepness of the isopycnals in this area suggests that there was an interaction between the two features. Overall, both satellite and in situ data indicated that the sampling stations included the coastal upwelling area and an ITE adjacent to the CUF (Figures 2a–2f), as detailed in Morales et al. (2017). Water mass distribution in the upper layer (0–100 m depth) for the CUF stations (Stations 5–7 and 16–18) and those nearest to it in the coastal (Stations 4 and 15) and oceanic (Stations 8 and 19) directions are represented in Figure 3. Both the ESSW and SAAW masses were detected (Figure 3). On the coastal side, the ESSW was dominant below 30 m depth, and the SAAW was dominant above it. In the CUF area, the contribution of the SAAW was slightly higher and reached deeper (40 m depth), and the ESSW was dominant below it. On the oceanic side, the contribution of the SAAW was extended down to 80 m depth, whereas that of the ESSW was minimal.

The vertical structure (0–300 m depth) of the meridional geostrophic circulation during the cruise is shown in Figure 4. In the area immediately beyond the shelf-break zone (~100 km from the coast), a southward flow was dominant, with values of 0.2 m s^{-1} in the CUF area of the northern transect (Station 17) and maximum values (~0.4 m s^{-1}) on the oceanic side of the CUF in the southern transect (Stations 7–8) (Figures 4a and 4b). Offshore of this flow, in the area of ITE-CUF interaction, a change to a northward flow was detected in both transects (Stations 9–10 and 19–21), with velocities reaching up to 0.1 m s^{-1} in the stations closer to the ITE center in the northern transect (Stations 21–23) and a higher intensity (0.1–0.2 m s^{-1}) in the stations located in the southeastern edge of the eddy in the southern transect (Stations 9–10) (Figures 4a and 4b). This coastal flow configuration is consistent with the PCUC current observed and modeled in summer, reaching values close to ~0–0.5 m s^{-1} in the study region (Aguirre et al., 2012; Chaigneau et al., 2013; Vergara et al., 2016) and off Peru (Thomsen et al., 2016). In the case of ITEs in the HCS, values reported
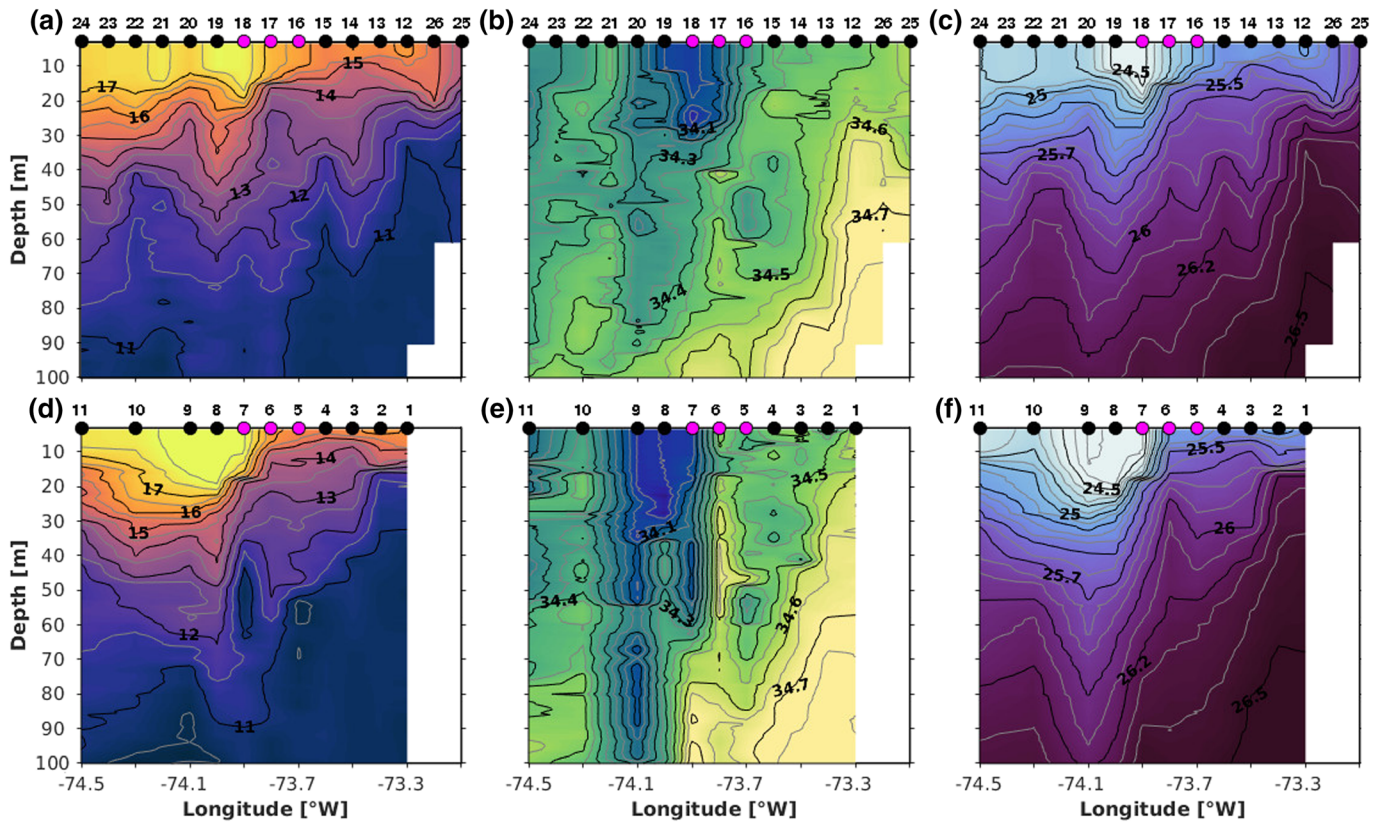
Figure 2. Vertical distribution of the oceanographic properties in the upper 100 m depth during the PHYTO-FRONT cruise. Temperature (°C), salinity, and potential density (kg m^{-3}) in the (a–c) northern and (d–f) southern transects. The colormap of each variable was done using the cmocean colormaps package (Thyng et al., 2016). Dots representation as in Figure 1.

previously (Thomsen et al., 2016) are not only similar to those in this study but also 1 order of magnitude higher than estimates for two eddies in the same region (0.02 m s^{-1}; Hormazabal et al., 2013). This is probably a result of eddy dynamics since Thomsen et al. (2016) also reported a time decrease (0.08 m s^{-1}) as they moved offshore.

3.2. Vertical Nutrient Gradients, Vertical Eddy Diffusivity, and Diapycnal Nutrient Fluxes

Vertical sections of macronutrient gradients in the layer immediately below the mixed layer (>10 m depth) during the cruise are shown in Figure 5, together with isopycnal distribution. These data are based on nutrient distribution in the upper layer (0–100 m depth) previously described in Morales et al. (2017). Phosphate and nitrate vertical gradients presented a similar pattern in both transects. Higher gradient values for phosphate (>0.03 μM m^{-1}) and nitrate (>0.5 μM m^{-1}) (Figures 5a, 5b, 5d and 5e) were detected in the 10–40 m layer of the CUF area (Stations 5–7 and 16–18) and deeper (30–40 m depth) in the ITE area (Stations 10–11 and 22–24). Gradient differences between the two transects were observed. In the northern transect, coastal stations (Stations 12, 25, and 26) displayed maxima for phosphate (>0.06 μM m^{-1}) and nitrate (>0.5 μM m^{-1}) (Figures 5a and 5b) in the 15–30 m layer. However, similar maxima for phosphate in the southern transect (Stations 1–4) were located at a shallower depth (10–15 m) and in stations closest to the CUF (Stations 3–4) and were accompanied by lower nitrate gradients (<0.5 μM m^{-1}) (Figures 5d an 5e). In the ITE-CUF interaction zone (Stations 9 and 20), low values for both phosphate and nitrate gradients were found in the whole water column, except for a localized maximum in nitrate at ~30 m depth in the northern transect (Figures 5a, 5b, 5d, and 5e). The silicate vertical gradients were relatively similar in the CZ and CUF areas of both transects and ranged between 0.1 and 1.0 μM m^{-1} in the 15–40 m layer; localized gradient maxima (>0.5 μM m^{-1}) were found in the 15–30 m layer in the CZ and CUF areas in the northern (Stations 12 and 16) and southern (Stations 3 and 5–6) transects. The lowest values were detected in the area
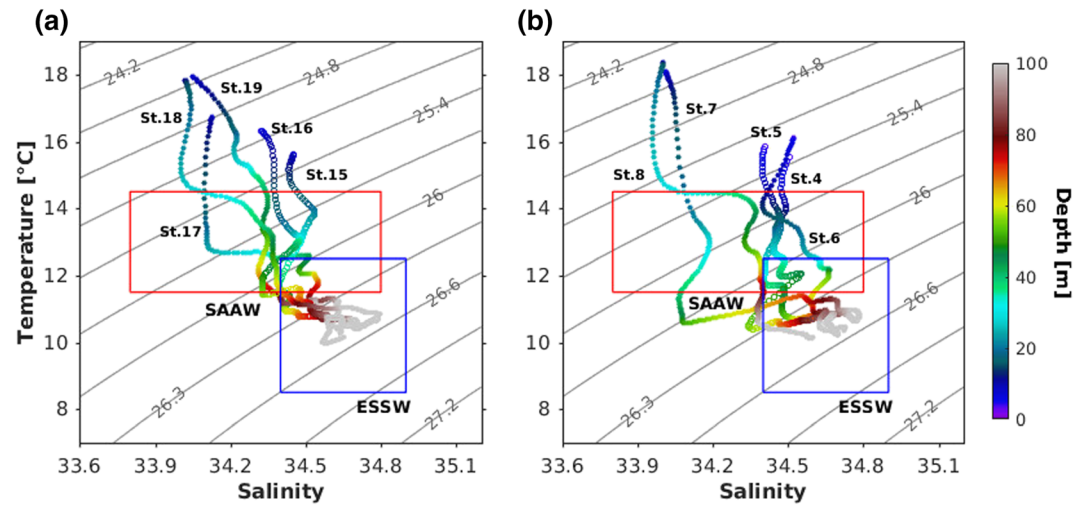
Figure 3. *T-S* diagrams of the upper 100 m depth for the stations located in the CUF area (Stations 5–7 and 16–18) and for those nearest to it in the coastal (Stations 4 and 15) and oceanic (Stations 8 and 19) directions, in the (a) northern and (b) southern transects of the PHYTO-FRONT cruise. The colors represent depth. The blue and red rectangles indicate the typical temperature-salinity features of the Equatorial Subsurface Water (ESSW) and Subantartic Water (SAAW) masses, respectively. The rectangles displayed in situ and modeled values reported by Silva et al. (2009), Llanillo et al. (2012), and Vergara et al. (2016). ESSW: 8.5–12.5 °C, 34.4–34.9; SAAW: 11.5–14.5 °C, 33.8–34.8.

beyond the CUF toward the ITE, whereas moderate increases in the subsurface layer (30–40 m depth) of the ITE area were observed in both transects (Stations 11 and 22–24) (Figures 5c and 5f). In general, maxima in nutrient gradients were found shallower (~10–30 m) in the CZ and CUF areas and deeper (~30–40 m) toward the ITE area (Figure 5), with most of them being located in the layer corresponding to the 25.5 and 26 kg m^{-3} isopycnals. These isopycnals have been identified as those separating the dominant water masses in the upper layer of this region, SAAW and ESSW (Llanillo et al., 2012).

Estimates of diapycnal nutrient fluxes for phosphate, nitrate, and silicate, together with the depth of maximum K_z in each station, are shown in Figure 6. The maximum flux values, their location in depth, the indirect estimates of the vertical eddy diffusivity (K_z), and the respective nutrient gradient values are detailed in Table 1. In both transects, the highest K_z values were found in the CUF and ITE areas (~0.3–
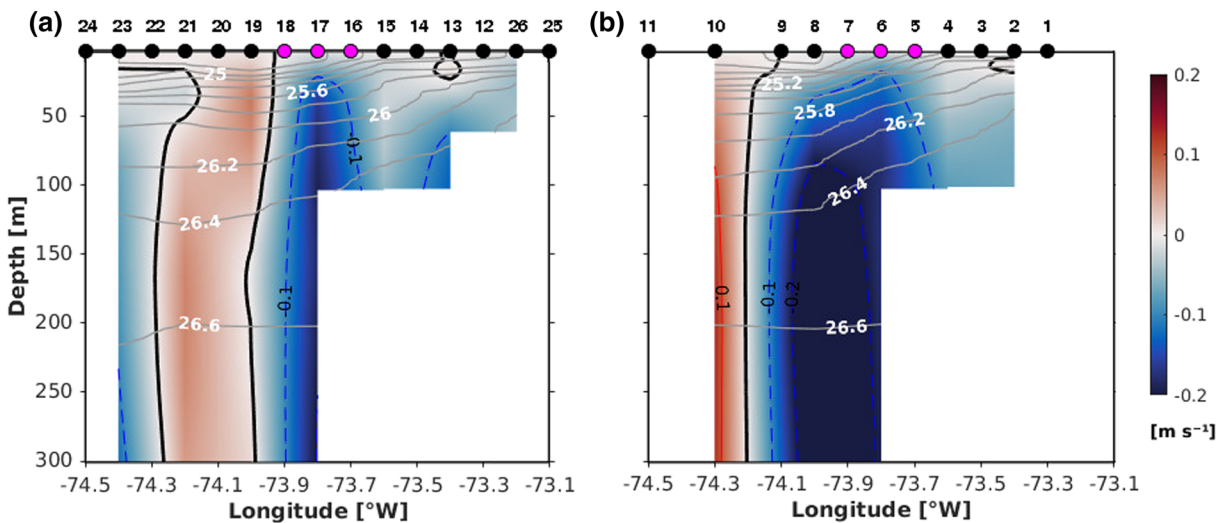

Figure 4. Meridional geostrophic velocity derived from conductivity, temperature, and depth from CTD casts in the upper 300 m depth water column for the (a) northern and (b) southern transects of the PHYTO-FRONT cruise. Positive (negative) velocity values represent a northward (southward) flow. The geostrophic velocity was computed from the geopotential anomaly relative to the sea surface. The thick black line represents the zero velocity contour, and the gray lines correspond to isopycnals; dots as in Figure 1.
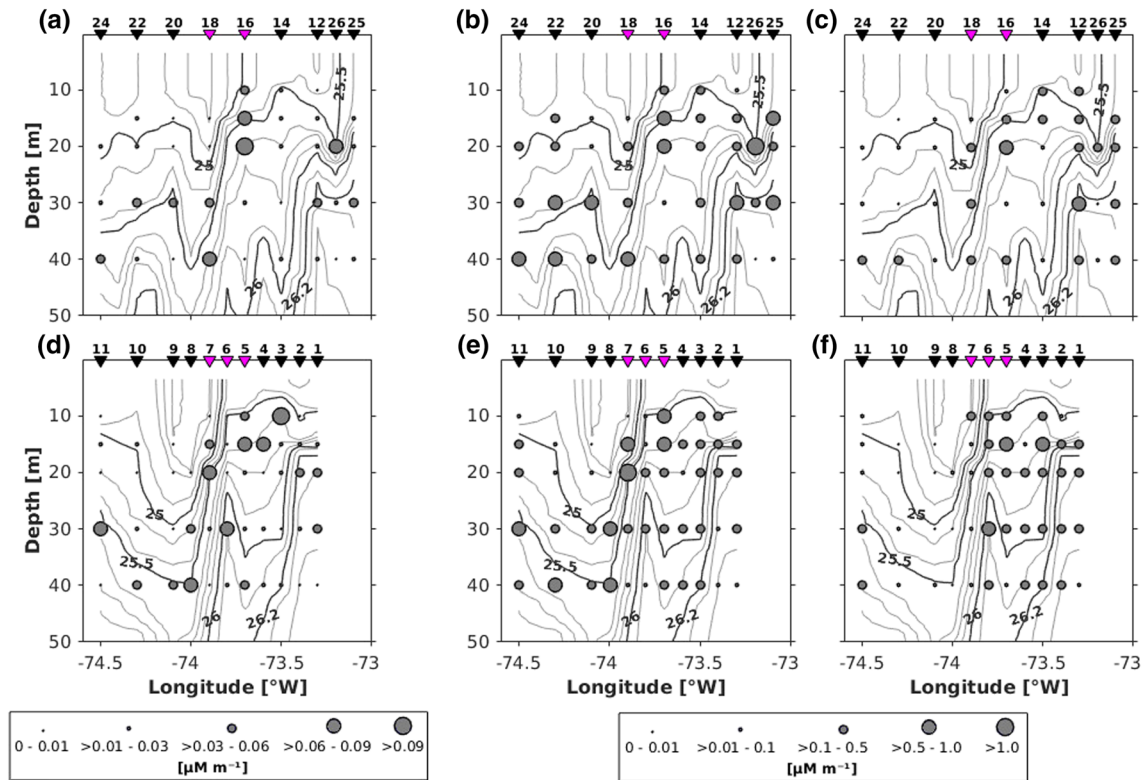
Figure 5. Vertical distribution of nutrient gradients ($\mu M\ m^{-1}$) in the upper 50 m depth for the (a–c) northern and (d–f) southern transects of the PHYTO-FRONT cruise. Gradients for (a, d) phosphate, (b, e) nitrate, and (c, f) silicate. The gray and black lines correspond to isopycnals, with potential density values less (greater) than 26.0 kg m^{-3} indicating the presence of the SAAW (ESSW) mass; triangles as in Figure 1.

$1.0 \times 10^{-4}\ m^2\ s^{-1}$ in the northern and ~ 1.2–$4.1 \times 10^{-4}\ m^2\ s^{-1}$ in the southern). Additionally, K_z was high in the CZ in the southern transect (Station 1; $\sim 2.8 \times 10^{-4}\ m^2\ s^{-1}$) and in the coastal station nearest to the CUF in the northern transect (Station 14; $\sim 0.7 \times 10^{-4}\ m^2\ s^{-1}$). Regarding nutrient fluxes, those of phosphate and nitrate were similar, and maximum values were observed in the southern transect, compared to the northern one. The highest values for phosphate ($>0.1\ mmol\ m^{-2}\ day^{-1}$) and nitrate ($>1\ mmol\ m^{-2}\ day^{-1}$) in the northern transect (Figures 6a and 6b) were found at a shallow depth (15–20 m) in both the CUF (Station 16) and ITE (Station 22) areas and also deeper (40 m) in the ITE area (maximum in nitrate flux: $>4.0\ mmol\ m^{-2}\ day^{-1}$). In contrast, the silicate flux (Figure 6c) displayed a single maximum ($>1\ mmol\ m^{-2}\ day^{-1}$) at depth (40 m) in the ITE area, with the rest displaying lower values ($<0.5\ mmol\ m^{-2}\ day^{-1}$). In the southern transect, maxima in phosphate ($>1.0\ mmol\ m^{-2}\ day^{-1}$) and nitrate ($>10\ mmol\ m^{-2}\ day^{-1}$) fluxes (Figures 6d and 6e) were found at a shallow depth (15 m) in the CUF area (Station 5), and high values (>0.5 and $>4.0\ mmol\ m^{-2}\ day^{-1}$, respectively) were also located deeper (>30 m) in the CZ and ITE areas (Stations 1 and 10–11). Silicate fluxes (Figure 6f) were also highest ($>10\ mmol\ m^{-2}\ day^{-1}$) in the CUF area (15 and 40 m, Stations 5–6) and moderate (1.0 to $<10\ mmol\ m^{-2}\ day^{-1}$) at 30 m depth in the CZ and ITE areas (Stations 1 and 11).

Since diapycnal nutrient flux depends on both nutrient gradients and K_z, their relative contribution to flux estimates in the CTZ is analyzed (Figure 7). It is to be noted that the K_z values are presented in a $\log_{10}$ scale, and two extreme flux estimates in the higher range were removed from these analyses. In all the cases, nutrient fluxes displayed a relationship with K_z (Figures 7a–7c), expressed here as linear correlation coefficients ($0.42 < r < 0.54$, p values < 0.01). In contrast, such a relationship was not found between phosphate and nitrate fluxes and their gradients ($r < 0.20$; $p > 0.2$), though this was the case for silicate ($r = 0.63$; $p < 0.001$) (Figures 7d–7f). Overall, these data suggest that diapycnal mixing was an important process in the water column immediately below the mixed layer in the CTZ off Concepción.
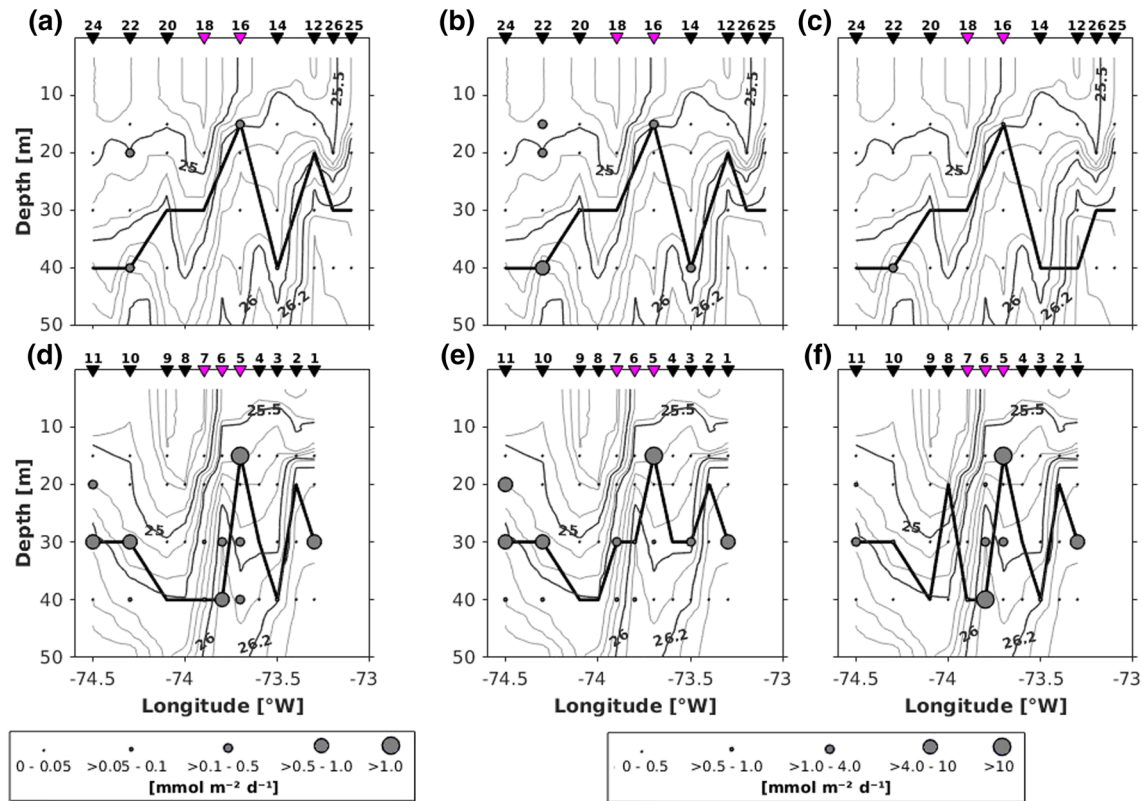
Figure 6. Vertical distribution of the upward diapycnal nutrient fluxes (mmol m^{-2} day^{-1}) in the upper 50 m depth for the (a–c) northern and (d–f) southern transects of the PHYTO-FRONT cruise. Fluxes for (a, d) phosphate, (b, e) nitrate, and (c, f) silicate. Thick black lines indicate the depth at which the maximum in each nutrient flux in each sampling station was detected. Lines and triangles as in Figure 5.

3.3. Total and Size-Fractionated Chl-a and Phytoplankton Cross-Shore Distribution

In order to evaluate how the phytoplankton size distribution compares with the estimated diapycnal nutrient fluxes, the depth of Chl-a maxima in each fraction size and the spatial distribution of total and microphytoplankton Chl-a concentrations are displayed in Figure 8; isopycnals and the depth of the mixed layer and that of the maxima in nitrate flux are also included. Maximum values in microphytoplankton, nanophytoplankton, and picophytoplankton Chl-a concentrations are detailed in Table 1, and their distribution has been previously described in Morales et al. (2017). Regarding the depth of the Chl-a maxima in each size fraction (Figures 8a and 8d), those in the microphytoplankton and nanophytoplankton fractions displayed a similar pattern, being located at a shallower depth (<20 m) in the CZ and deeper toward offshore. In contrast, those of picophytoplankton were all located at a shallow depth. The vertical distribution of Chl-a maxima in the larger-size fractions, especially those of the microphytoplankton, followed closely those of maxima in diapycnal nitrate flux. Maxima in total Chl-a (>3 mg m^{-3}) were detected in the surface layer (<20 m depth) of the CUF area (Stations 5 and 16), together with moderate values (~1–3 mg m^{-3}) in the surface layer of the CZ and at the subsurface (~20–30 m depth) in the ITE area (Stations 10–11 and 20–24). The highest values were all located at or above the depth of maximum diapycnal nitrate flux and above or below the mixed layer (Figures 8b and 8e). In contrast, maxima in microphytoplankton Chl-a were located only in the CUF (Stations 5 and 16) and ITE (Stations 10 and 22) areas, above and below the mixed layer in the CUF area and below it in the ITE area (Figures 8c and 8f) (Table 1). Overall, these results suggest that maxima in microphytoplankton Chl-a below the mixed layer are probably the result of vertical nutrient injections in the ITE-CUF zone.

Further, the spatial distribution of total microdiatom abundance and that of two numerically dominant diatom species (*Chaetoceros debilis* and *Pseudo-nitzschia pseudo-delicatissima*) were analyzed in combination with the depth of maxima in nitrate flux and of the mixed layer (Figure 9). It must be noted that

Table 1

Mixed Layer Depth (MLD; m), Maximum Diapycnal Nutrient Flux (mmol m^{-2} day^{-1}), and Vertical Nutrient Gradients (μM m^{-1}) for Phosphate, Nitrate, and Silicate, Vertical Eddy Diffusivity Coefficient (K_z; m^2 s^{-1}), and Maximum Values of Size-Fractionated (Microphytoplankton, Nanophytoplankton, and Picophytoplankton) Chl-a Values (mg m^{-3}) at Each Sampling Station During the PHYTO-FRONT Cruise

North transect

Variable 1	Variable 2	Station 25	Station 26	Station 12	Station 14	Station 16	Station 18	Station 20	Station 22	Station 24
	Zone	CZ	CZ	CZ	CZ	CUF	CUF	CUF	ITE	ITE
	Longitude (°W)	−73.1	−73.2	−73.3	−73.5	−73.7	−73.9	−74.1	−74.3	−74.5
MLD		13.5	19.0	10.5	10.5	10.5	15.5	12.5	14.0	19.0
Phosphate	Flux	0.02 (30)	0.01 (30)	0.01 (20)	0.08 (40)	0.21 (15)	0.04 (30)	0.04 (30)	0.26 (40)	0.01 (40)
	Gradient	0.0310	0.0250	0.0290	0.0135	0.0690	0.0310	0.0550	0.0300	0.0510
	K_z	0.09e−4	0.07e−4	0.02e−4	0.71e−4	0.35e−4	0.14e−4	0.09e−4	1.00e−4	0.03e−4
Nitrate	Flux	0.46 (30)	0.09 (30)	0.08 (20)	1.05 (40)	1.63 (15)	0.29 (30)	0.55 (30)	5.12 (40)	0.20 (40)
	Gradient	0.5940	0.1460	0.3480	0.1720	0.5330	0.2450	0.7100	0.5910	0.7200
	K_z	0.09e−4	0.07e−4	0.02e−4	0.71e−4	0.35e−4	0.14e−4	0.09e−4	1.00e−4	0.03e−4
Silicate	Flux	0.28 (30)	0.01 (30)	0.05 (40)	0.33 (40)	0.85 (15)	0.24 (30)	0.07 (30)	2.53 (40)	0.06 (40)
	Gradient	0.3590	0.0100	0.3460	0.0535	0.2780	0.2050	0.0865	0.2920	0.2060
	K_z	0.09e−4	0.07e−4	0.01e−4	0.71e−4	0.35e−4	0.14e−4	0.09e−4	1.00e−4	0.03e−4
Chl-a	Micro	0.30 (5)	1.63 (5)	1.34 (5)	0.58 (20)	13.74 (10)	1.30 (30)	1.23 (25)	1.99 (30)	0.90 (30)
	Nano	0.67 (0)	0.58 (5)	1.44 (20)	1.19 (15)	2.89 (10)	0.35 (15)	1.36 (30)	0.66 (30)	0.55 (30)
	Pico	0.38 (5)	0.24 (0)	0.69 (15)	0.53 (10)	0.28 (10)	0.08 (10)	0.08 (5)	0.31 (20)	0.05 (10)

South transect

Variable 1	Variable 2	Station 1	Station 2	Station 3	Station 4	Station 5	Station 6	Station 7	Station 8	Station 9	Station 10	Station 11
	Zone	CZ	CZ	CZ	CZ	CUF	CUF	CUF	ITE	ITE	ITE	ITE
MLD		12.5	11.5	11.5	12.5	11.0	11.5	11.0	17.5	14.5	12.0	10.5
Phosphate	Flux	0.83 (30)	0.01 (20)	0.06 (40)	0.02 (30)	2.25 (15)	0.62 (40)	0.08 (40)	0.03 (40)	0.02 (40)	0.53 (30)	0.66 (30)
	Gradient	0.0335	0.0480	0.0210	0.0180	0.0680	0.0180	0.0080	0.0720	0.0350	0.0150	0.0620
	K_z	2.86e−4	0.03e−4	0.32e−4	0.12e−4	3.83e−4	4.02e−4	1.22e−4	0.05e−4	0.06e−4	4.12e−4	1.24e−4
Nitrate	Flux	9.06 (30)	0.11 (20)	3.23 (30)	0.35 (30)	19.11 (15)	0.90 (30)	1.31 (30)	0.44 (40)	0.08 (40)	8.65 (30)	8.01 (30)
	Gradient	0.3670	0.4740	0.1060	0.3440	0.5780	0.2320	0.4800	0.9050	0.1360	0.2430	0.7480
	K_z	2.86e−4	0.03e−4	3.53e−4	0.12e−4	3.83e−4	0.45e−4	0.32e−4	0.05e−4	0.06e−4	4.12e−4	1.24e−4
Silicate	Flux	6.22 (30)	0.09 (20)	0.74 (40)	0.19 (30)	23.07 (15)	10.12 (40)	0.77 (40)	0.06 (20)	0.06 (40)	1.00 (30)	1.63 (30)
	Gradient	0.2520	0.3720	0.2710	0.1920	0.6980	0.2910	0.0730	0.0900	0.1120	0.0280	0.1520
	K_z	2.86e−4	0.03e−4	0.32e−4	0.12e−4	3.83e−4	4.02e−4	1.22e−4	0.08e−4	0.06e−4	4.12e−4	1.24e−4
Chl-a	Micro	0.26 (10)	0.54 (5)	0.15 (15)	0.62 (20)	2.25 (10)	0.25 (10)	0.24 (10)	0.10 (30)	0.16 (30)	1.01 (20)	1.09 (30)
	Nano	0.97 (5)	0.94 (5)	1.37 (5)	0.94 (5)	1.23 (10)	1.64 (10)	0.95 (30)	0.95 (30)	0.48 (30)	1.10 (20)	1.09 (30)
	Pico	0.68 (10)	1.05 (0)	1.02 (0)	0.40 (0)	0.59 (5)	0.48 (5)	0.29 (20)	0.09 (10)	0.06 (10)	0.06 (5)	0.31 (5)

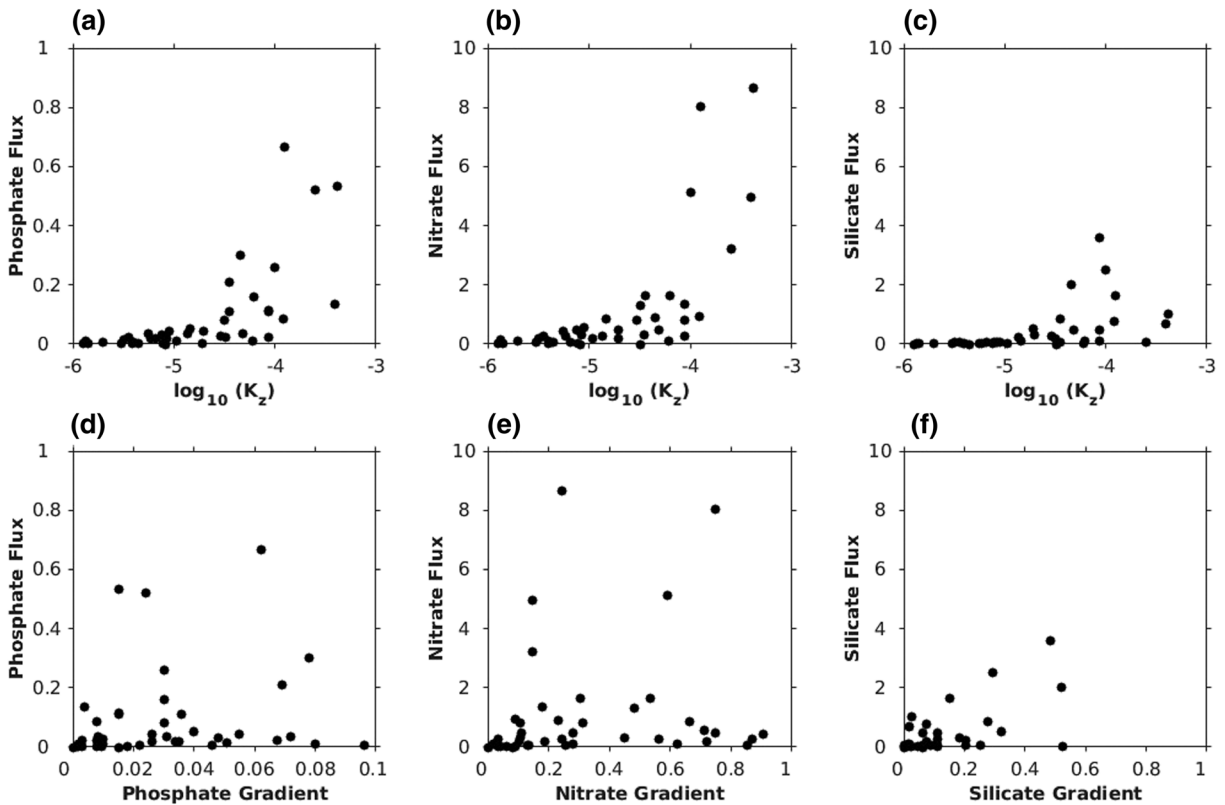*Note.* The depth (m) of Chl-a maxima is in parentheses.

Figure 7. Relationship between nutrient (phosphate, nitrate, and silicate) flux and the two variables that define it, (top) vertical eddy diffusivities or K_z coefficient and (bottom) nutrient gradients in the CUF and ITE areas for both transects of the PHYTO-FRONT cruise. Nutrient flux units in mmol m^{-2} day^{-1}, nutrient gradients in μM m^{-1}, and $\log_{10}(K_z)$ units in m^2 s^{-1}.

dominant diatoms are included in both size classes since most of them form chains (micro-) before or after evolving as single cells (nano-) in the region (Morales et al., 2017). The highest values of total abundance were detected above and below the mixed layer depth in the CUF and ITE areas of the transects (Figures 9a and 9d), coinciding with maxima in microplankton Chl-a (Figures 8c and 8f); in contrast, their abundance was lower, and the maxima were found above the mixed layer depth in the CZ. Primary maxima in the abundance of the coastal diatom *Ch. debilis* were observed in the CUF area and secondary ones in the ITE area in the northern transect. In the southern transect, abundances were lower, and secondary maxima were located in the subsurface of the ITE area (Figures 9b and 9e). Primary maxima in the abundance of the oceanic diatom *P. pseudo-delicatissima* were located in the ITE area in both transects and a secondary one in the CUF area of the northern transect, most of them below the mixed layer depth (Figures 9c and 9f). Overall, microplankton Chl-a and the abundance of microdiatoms were maxima in the areas of highest diapycnal nitrate (and phosphate) flux. Although the distribution of maxima in silicate flux was slightly different from these other two nutrients (Figure 6), maxima in the CUF and ITE areas were relatively similar for all of them, so that the results based on nitrate apply to the other two nutrients.

Altogether, diapycnal nutrient fluxes in the CTZ were the highest in the southern transect compared to those in the northern one (Figure 6), and the reverse is true for both microphytoplankton Chl-a (Figures 8c and 8f) and total microdiatom abundance (Figures 9a and 9d). This difference could be related to an intense silicate deficit (N/Si ratios >3) in the water column of the southern transect, associated with an intrusion of Si-poor waters through the southern edge of the ITE (Morales et al., 2017). In addition, a higher abundance of the coastal diatom species *Ch. debilis* in the CUF area of the northern transect, compared to the southern one, may also be related to their initial entrainment in coastal waters advected offshore through mesoscale and/or submesoscale processes, but which may subsist on vertical nutrient injections.
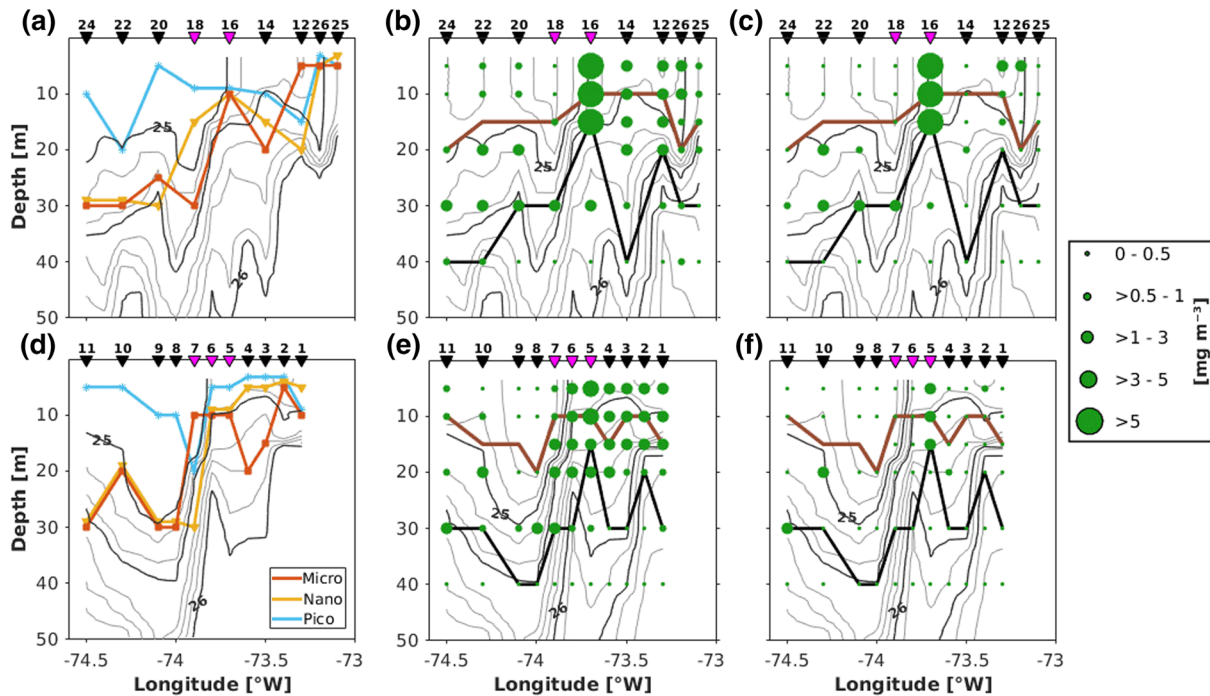
Figure 8. Spatial distribution of phytoplankton size-fractionated biomass (Chl-a) in the upper 50 m depth for the (a–c) northern and (d–f) southern transects of the PHYTO-FRONT cruise. (a, d) Depth of maximum Chl-a size fraction at each station and distribution of (b, e) total and (c, f) microphytoplankton Chl-a values. The brown line indicates the mixed layer depth obtained by using $\Delta\rho = 0.03$ kg m^{-3} following the procedure of de Boyer Montégut et al. (2004). The gray lines correspond to isopycnals, and the thick black line indicates the depth of nitrate flux maxima. Triangles as in Figure 1.

4. Discussion

4.1. Thorpe Scale Method to Estimate Vertical Eddy Diffusivity

The use of density overturns in the water column to estimate the dissipation rate of turbulent kinetic energy assumes a linear relationship between the Thorpe length scale and the Ozmidov length scale, with the latter interpreted as the vertical size of the largest eddies that can overturn (Ozmidov, 1965). Mater et al. (2015), through a detailed analysis of in situ data from different regions (Luzon Strait and Atlantic Ocean), found that the Thorpe scale method in comparison with microstructure profiler data overestimates the dissipation rates when the vertical size of the overturns is too large, that is, when the Thorpe scale is larger than the Ozmidov scale. In agreement with this, Scotti (2015) concluded that in cases of convective-driven mixing (i.e., when the mixing is driven by the available potential energy of the mean flow), the Thorpe scale is larger than the Ozmidov scale and the Thorpe method tends to overestimate the dissipation rate and turbulent mixing. In contrast, the Thorpe scale is equivalent to the Ozmidov scale in cases of shear-driven flows, which means that the method is appropriate to estimate vertical eddy diffusivities when the energy for mixing comes from the kinetic energy associated with the mean flow. In summary, the performance of the Thorpe scale method based on CTD data, compared to direct estimates obtained from direct microstructure measurements, will depend on the environmental conditions and the energetics for mixing (Mater et al., 2015; Park et al., 2014; Scotti, 2015). In regions of high stable stratification and diapycnal turbulent mixing in deep waters (>200 m), both direct and indirect methods have been reported to have a good agreement (Ferron et al., 1998; Klymak et al., 2008). In contrast, in regions under extreme environmental conditions and low stratification (e.g., Southern Ocean and the Drake Passage), as well as under conditions of double-diffusive convection events (diffusive-layering events) produced by fresh, cold waters overlying salty, warm waters (e.g., fjord regions), dissipation rates of turbulent kinetic energy have been reported to be overestimated by 1 to 2 orders of magnitude when using the CTD-based Thorpe scale method (Frants et al., 2013; Pérez-Santos et al., 2014).

In our study, no direct measurements of turbulence dissipation rates through a microstructure profiler were available. Instead, the Thorpe length scale to estimate K_z was applied to CTD data, assuming a conceptual
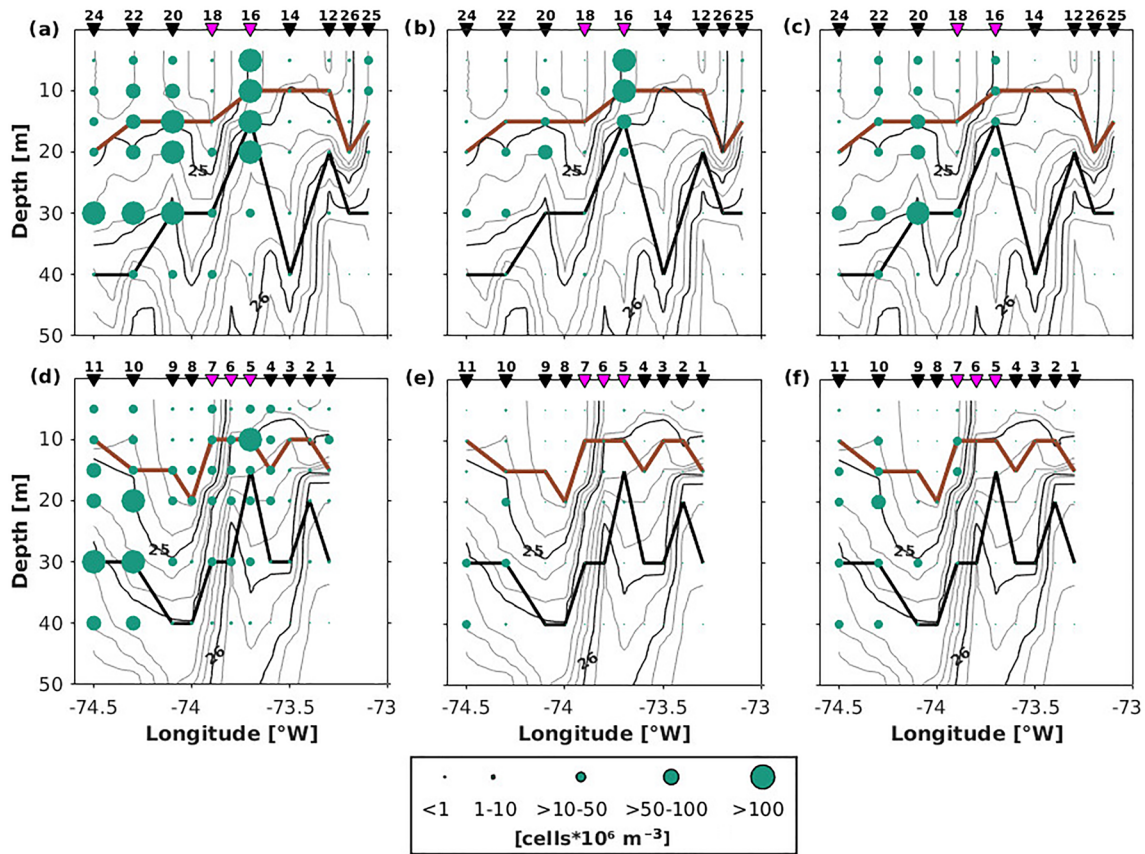
Figure 9. Spatial distribution of diatom abundance (cells × 10^6 m^{-3}) in the upper 50 m depth for the (a–c) northern and (d–f) southern transects of the PHYTO-FRONT cruise. (a, d) Total diatom abundance, (b, e) coastal species *Chaetoceros debilis*, and (c, f) oceanic species *Pseudo-nitzschia pseudo-delicatissima*. Lines and triangles as in Figure 8.

model where a combination of two prominent mechanisms, frontogenesis and symmetric instability, was taking place. Under this assumption, the following processes could have been occurring: (i) the mesoscale velocity field of the ITE might have contributed to enhance the cross-frontal density gradient, compressing and steepening the isopycnals in the offshore side of the CUF and, thereby, increasing the vertical shear and the turbulence in the area; and (ii) an intensification of the surface currents produced by the ITE-CUF interaction might lead to submesoscale shear instabilities, allowing the extraction of kinetic energy from the geostrophic flow and turning it into turbulence and mixing. In both cases, the energetics for mixing would come from the kinetic energy associated with the mean flow, cases in which the Thorpe scale is equivalent to the turbulent component of the Thorpe displacements, so that indirect estimates with the Thorpe method become adequate in the assessment of turbulent diapycnal mixing (Scotti, 2015). The two mechanisms described above have been previously shown to be interacting in the upper layer (<200 m depth) of the northern region in the HCS (upwelling system off southern Peru), where intense mesoscale and submesoscale activity was registered with in situ glider monitoring (Pietri et al., 2013). In addition, inertial or symmetric instability in the upper layer (<100 m) has been detected through modeling the ITE formation process in the southern region of the HCS (upwelling system off central southern Chile) (Contreras et al., 2019). However, the specific contributions of each of these or other mechanisms to turbulence and/or diapycnal mixing in the HCS remain to be investigated.

Studies focused on the comparison and validation of indirect estimates of vertical diffusivities from the Thorpe method with those directly obtained from microstructure profiler have not been reported for the HCS EBUS. However, during an oceanographic campaign (Humboldt-2009 Bio-Hesperides) conducted off Chile (24–42°S), both types of measurements (CTD density overturns and microstructure profiles) were performed at four sampling stations closest to the CZ (<100 km offshore). In all the cases and in the upper 450 m

depth, the data available indicate that both methods matched in the areas of maximum and minimum K_z, with values oscillating between ~10^{-6} and 10^{-4} m^2 s^{-1} (Hormazabal, unpublished data). Our K_z estimates are within the upper range of these data (~10^{-4} m^2 s^{-1}; Table 1). Further, they agree with direct measurements in the CC EBUS (e.g., Hales et al., 2005; Li et al., 2012). In summary, the Thorpe scale method using CTD data is still a useful method for the assessment of turbulent mixing (e.g., Correa-Ramirez et al., 2019), whenever the underlying processes that generate mixing are considered (Mater et al., 2015; Scotti, 2015). Since mixing processes are a key factor controlling nutrient fluxes in the sunlit layer and hence have an important role in the submesoscale variability of phytoplankton communities (D'Asaro et al., 2011; de Verneil et al., 2019), future studies in the HCS region would benefit from using multidisciplinary approaches and multiple sampling techniques, to obtain high-spatiotemporal-resolution physical, biogeochemical, and biological data.

4.2. Diapycnal Nutrient Fluxes in Areas of Intense Mesoscale and Submesoscale Activity in EBUSs

Most studies on vertical nutrient fluxes in EBUS regions refer only to nitrate flux. In the case of frontal zones, elevated mixing has been registered with a microstructure profiler in a front located in the CC, with estimates of turbulent nitrate fluxes in the order of 0.1 to 0.3×10^{-5} mmol m^{-2} s^{-1} (0.08 to 0.26 mmol m^{-2} day^{-1}) (Johnston et al., 2011). This range is in the lower limit of the nitrate flux maxima per station in our study (0.08–19.1 mmol m^{-2} day^{-1}; Table 1). However, the latter were derived from in situ nutrient distribution, whereas in the former, they were estimated from nutrient-density correlations, implying a greater degree of uncertainty in the comparison. In addition, the above CC estimates are between 1 and 2 orders of magnitude lower, compared to direct microstructure measurements in a shelf-break front off New England (western North Atlantic), which reached 6×10^{-5} mmol m^{-2} s^{-1} (5.2 mmol m^{-2} day^{-1}) (Hales et al., 2009), and in CC fronts, with reported values of 0.0001 mmol m^{-2} s^{-1} (8.64 mmol m^{-2} day^{-1}) (Hales et al., 2005) and up to 6.9 mmol m^{-2} day^{-1} (Li et al., 2012). In summary, estimates available for the CC are in the middle range of our maximum estimates of diapycnal nitrate flux per station.

Differences in the nitrate fluxes detailed above could be associated with differences in the energy sources for turbulence and with the impact of front interaction with other mesoscale or submesoscale features. Without a certainty on the specific contribution of different mechanisms in generating higher or lower nitrate flux values, we speculate that changes in the mechanisms will also imply changes between the reported nitrate fluxes in the CC front and with our estimates. In the CC front, Johnston et al. (2011) proposed that turbulent mixing was due to the increased shear by the reflected near-inertial internal waves on the dense side of the front and the frontogenesis produced by near-surface currents along the front. However, the mean shear was not as high as the authors expected from frontogenesis or straining, resulting in lower diapycnal nitrate flux. Hales et al. (2005) and Li et al. (2012) found the nitrate flux estimates are similar but the physical dynamics appear to have been different. In the first case, high nitrate content at the front was due to upwelling transport along isopycnal surfaces, and the role of turbulent mixing across isopycnals was to maintain the upward injection of nitrate, implying that nutrient gradient was of greater importance in the diapycnal nitrate flux. In the second case, an intense cross-isopycnals vertical mixing due to density instabilities by the Ekman flow was reported, accompanied by an ageostrophic cross-frontal circulation and symmetric instabilities. The three latter mechanisms can simultaneously promote intense turbulent mixing (D'Asaro et al., 2011; Franks & Walstad, 1997; Thomas & Taylor, 2010). In our case, we suggest that symmetric instabilities as a source of cross-isopycnals mixing and the ageostrophic circulation as a consequence of frontogenesis were taking place, with the latter as the intensification of the CUF due to the acceleration of the geostrophic flow by the ITE. Our maximum diapycnal nitrate flux estimate is almost double that reported by Li et al. (2012), despite the similarity in the mechanisms that may have been involved. On this basis, we suggest that the ITE-CUF interaction in our study acts as a potential amplifier of diapycnal mixing through an acceleration of the geostrophic flow by the ITE, also enhancing the nitrate flux toward the upper layer.

In the case of eddies in EBUSs, no records on diapycnal nutrient fluxes have been reported yet, to the best of our knowledge. As a reference on an oceanic mesoscale eddy in the North Atlantic, diapycnal nitrate and phosphate fluxes (1.8 and 1.25 mmol m^{-2} day^{-1}) at the base of the mixed layer are in the lower range of our maximum estimates per station (20 and 2.25 mmol m^{-2} day^{-1}, respectively). The study concludes that the contribution of vertical turbulence to nutrient delivery was lower, compared to that of advective processes (Law et al., 2001). Likewise, Zhang et al. (2018) used a long-term high-resolution simulation for the

Gulf Stream region and found a nitrate flux of ~3 mmol m^{-2}day^{-1} within anticyclonic mesoscale eddies. The authors argued that such flux was mainly related to eddy-wind interactions inducing Ekman pumping and enhanced vertical advective fluxes at the base of the photic zone. Besides the potential for an upward advective flux of nutrients, downward vertical velocities have also been found along isopycnals in upwelling fronts and in the periphery of mesoscale eddies, as well as in eddy flow fields through convergence and/or frontogenesis. This generates subsurface intrusions of surface water properties and a downward transport of Chl-a and particulate organic carbon (Callbeck et al., 2017; Mahadevan & Tandon, 2006; Omand et al., 2015). Recently, de Verneil et al. (2019) suggested that mixing along isopycnals would tend to erase localized phytoplankton patches, instead of creating them or producing high phytoplankton biomass across different isopycnals. This pattern would imply that a distinction between the two vertical mixing mechanisms (along isopycnals and across isopycnals) could be made.

Advective flux of nutrients was not quantified in our study due to the poor resolution in the velocity field in all directions (zonal, meridional, and vertical), but it could have been involved as well. At the same time, the suggested mechanisms as energy sources for vertical mixing are not exclusive to turbulent diapycnal mixing. We can only interpret that the estimated density overturns in the water column using K_z are associated with cross-isopycnal (diapycnal) mixing. Nevertheless, K_z does not fully represent the 3-D submesoscale and mesoscale dynamics. In our study, nutrient fluxes toward the upper layer were found to be highly associated with the turbulent diapycnal mixing (Figure 7), leading us to argue that this mechanism is contributing to nutrient injections toward the upper layer in the central southern HCS, as it happens in the CC (Li et al., 2012). No doubt, future studies are needed to assess the specific or relative contribution of different physical mechanisms to understand their impacts on mesoscale and submesoscale variability in nutrients and phytoplankton communities in EBUSs.

4.3. Diapycnal Mixing as a Mechanism Contributing to Phytoplankton Increases and Community Size Structure in the CTZ of EBUSs

The mechanisms leading to changes in phytoplankton biomass/production and community structure in mesoscale and submesoscale features is a complex subject of analysis due to the transient nature of such features, the continuous cascading of energy to and from these scales, the simultaneous occurrence of different physical processes within these features (e.g., downwelling, upwelling, stirring, and trapping), regional differences in water mass composition, and nutrient content associated with them. The biological and ecological dynamics (e.g., growth, grazing, and symbiosis) taking place at these scales (Lévy et al., 2018; Mahadevan, 2016; McGillicuddy, 2016) also contribute in this regard. An understanding of the mechanisms involved becomes more complex in the case of mesoscale and submesoscale features adjacent to wind-driven coastal upwelling zones in EBUSs (Chenillat et al., 2015; Nagai et al., 2015; Stramma et al., 2013). This is more so in the case of adjacent interacting features, such as eddy-eddy and eddy-front interactions (Harrison & Siegel, 2014; Krause et al., 2015). In the case of EBUSs, observational studies on the physical mechanisms that have an impact on the mesoscale and submesoscale variability of phytoplankton communities are still very limited and those available refer to a single type of feature and only to total Chl-a variability (de Verneil et al., 2019; Johnston et al., 2011; Li et al., 2012; Pietri et al., 2013) or productivity (Brzezinski & Washburn, 2011). In this context, the present study explored only one of the physical mechanisms leading to submesoscale and microscale vertical injection of nutrients toward the upper sunlit layer, the influence of diapycnal mixing on nutrient fluxes, and, thereby, on phytoplankton biomass and size structure distributions in the southern HCS. We recognize that diapycnal mixing might take place in combination with other processes, simultaneously or in sequence, to modulate nutrient distribution and phytoplankton communities in the HCS, so that further investigations on the contribution of diverse processes will be required to complete the picture presented here.

To put our results in perspective, we summarize below the current knowledge of the mechanisms driving phytoplankton biomass and/or size variability in EBUSs. In the case of frontal areas in coastal and CTZ regions (i.e., upwelling fronts, shelf-break fronts, and CTZ deep fronts), several mechanisms can contribute to increases observed in phytoplankton, including physical and biological processes. Among the physical mechanisms, turbulent mixing and water mass convergence have been identified as promotors of local phytoplankton growth and/or phytoplankton biomass accumulation in the CC EBUS (de Verneil et al., 2019; Hales et al., 2005; Johnston et al., 2011; Krause et al., 2015; Li et al., 2012; Taylor et al., 2012). As for the

phytoplankton community structure in EBUS frontal areas, our results are similar to those obtained in the CC CTZ, where an enhancement of phytoplankton biomass and a size shift toward larger cells were found at the front (Taylor et al., 2012). In the case of EBUS eddies, enhanced phytoplankton biomass and/or primary productivity in them have been shown to be influenced by enhanced vertical nutrient supply associated with an uplift of isopycnal surfaces (eddy pumping or other), convergence, and/or by occasional entrainment of phytoplankton and nutrients from the advection of water upwelled (eddy trapping) in the CZ (Brzezinski & Washburn, 2011; Chenillat et al., 2015). As for the effects of eddy dynamics on phytoplankton size structure, to the best of our knowledge, in situ variability has not been reported for EBUSs yet, but only on satellite-derived size structure (Corredor-Acosta et al., 2018). The latter results suggest that microphyto-plankton was an important fraction of total Chl-a in the early stages of the eddy lifetime, when they are closer to the CZ, but no mechanisms to explain this pattern were assessed.

Based on the results in Morales et al. (2017), front-eddy interactions in EBUSs could contribute to sustain phytoplankton growth in the CTZ through localized upward injections of nutrients, combined with ITE-induced horizontal advection of coastal waters and vertical nutrient inputs to the surface layer. Results in the present study suggest that maxima in microphytoplankton Chl-a below the mixed layer are most probably the result of localized vertical nutrient injections in the ITE-CUF zone (Figures 8 and 9), especially considering that nutrients were nearly depleted at a shallow depth (<20 m) in this zone. The mechanisms leading to similar maxima in the mixed layer in the CUF area are less clear (e.g., biomass accumulation by advection from the CZ and subsequent subduction versus in situ growth stimulated by vertical nutrient injections). However, the fact that dominant coastal and oceanic diatoms (*Ch. debilis* and *P. pseudo-delicatissima*, respectively) were most abundant in the ITE and CUF areas than in the CZ (Figure 9) suggests that there was a cross-shore mixing of coastal and oceanic species at the sampling time (see also Morales et al., 2017), in contrast to an accumulation of coastal phytoplankton biomass at the CUF. Nevertheless, the latter process can occur under conditions different from the ones here, as suggested by the distribution of size-fractionated Chl-a in the CZ and CTZ in the same area of study (Morales et al., 2012). At the same time, fronts and eddies include both upwelling and subduction submesoscale processes, so that a combination of diverse mechanisms can be in place to influence phytoplankton distribution and production. The mechanisms involved cannot be disentangled if measurements of primary production rates, as well as of other planktonic metabolic rates in the region, are included and regularly monitored in both the upwelling CZ and the CTZ in EBUSs. Future time series studies using fine-scale sampling methods combined with traditional approaches would be most important in resolving the mechanisms that contribute to the high productivity of the HCS, other than wind-driven coastal upwelling, and how they might be affected by regional- and large-scale oceanographic variability and vice versa.

5. Conclusions

EBUSs are regions of intense mesoscale and submesoscale activity, such as CUFs, filaments, surface eddies and ITEs, and all these features have an important impact on phytoplankton distribution, community structure, and ecosystem dynamics. This study focuses on the role of small-scale turbulent diapycnal mixing in modulating phytoplankton size distribution in a zone of ITE-CUF interaction in the HCS off central southern Chile. Our results suggest that maximum values in vertical nutrient fluxes took place in the CUF and ITE areas in association with maxima diapycnal mixing, favoring the competitive advantage that larger phytoplankton cells (diatoms) have compared to that of small sizes. In the CUF area, maximum abundance of coastal diatom taxa was found in association with higher diapycnal nutrient fluxes below the mixed layer depth. These findings suggest that turbulent diapycnal mixing in zones of intense mesoscale and submesoscale activity, including ITE-CUF interactions, can promote the presence of large phytoplankton cells and could be an important mechanism to support primary productivity in EBUSs.

Conflict of Interest:

The authors declare that the research was conducted in the absence of any commercial or financial relationships that could be considered as a potential conflict of interest.

Author Contributions:

Data collection during the PHYTO-FRONT cruise was carried out by C. E. M., V. A., L. P. V., S. H., and A. C. A. In situ size-fractionated Chl-a and diatom abundance analysis was done by V. A., C. E. M., and A. C. A. Thorpe scale method and diapycnal nutrient fluxes analysis was performed by L.P.V., A.R.S., C.E. M., and A.C.A. Manuscript writing was the responsibility of A. C. A. and C. E. M., with input from all coauthors.

References

Aguirre, C., Pizarro, O., Strub, P. T., Garreaud, R., & Barth, J. A. (2012). Seasonal dynamics of the near-surface alongshore flow off central Chile. *Journal of Geophysical Research*, *117*, C01006. https://doi.org/10.1029/2011JC007379

Anabalón, V., Morales, C. E., González, H. E., Menschel, E., Schneider, W., Hormazabal, S., & Escribano, R. (2016). Micro-phytoplankton community structure in the coastal upwelling zone off Concepción (central Chile): Annual and inter-annual fluctuations in a highly dynamic environment. *Progress in Oceanography*, *149*, 174–188. https://doi.org/10.1016/j.pocean.2016.10.011

Arcos-Pulido, M., Rodríguez-Santana, A., Emelianov, M., Paka, V., Arístegui, J., Benavides, M., et al. (2014). Diapycnal nutrient fluxes on the northern boundary of Cape Ghir upwelling region. *Deep Sea Research Part I: Oceanographic Research Papers*, *84*, 100–109. https://doi.org/10.1016/j.dsr.2013.10.010

Atlas, E., Hager, S., Gordon, L., & Park, P. (1971). *A practical manual for use of the Technicon Autoanalyzer in sea water nutrient analyses (Tech. Rep. 215)*. Corvallis, OR: Department of Oceanography, Oregon State University.

Brink, K. H., & Cowles, T. J. (1991). The coastal transition zone program. *Eos, Transactions of the American Geophysical Union*, *69*(27), 698–707. https://doi.org/10.1029/88EO01006

Brown, S. L., Landry, M. R., Selph, K. E., Yang, E. J., Rii, Y. M., & Bidigare, R. R. (2008). Diatoms in the desert: Plankton community response to a mesoscale eddy in the subtropical North Pacific. *Deep Sea Research Part II: Topical Studies in Oceanography*, *55*(10-13), 1321–1333. https://doi.org/10.1016/j.dsr2.2008.02.012

Brzezinski, M. A., & Washburn, L. (2011). Phytoplankton primary productivity in the Santa Barbara Channel: Effects of wind-driven upwelling and mesoscale eddies. *Journal of Geophysical Research*, *116*, C12013. https://doi.org/10.1029/2011JC007397

Callbeck, C. M., Lavik, G., Stramma, L., Kuypers, M. M., & Bristow, L. A. (2017). Enhanced nitrogen loss by eddy-induced vertical transport in the offshore Peruvian oxygen minimum zone. *PLoS ONE*, *12*(1), e0170059. https://doi.org/10.1371/journal.pone.0170059

Capet, A., Mason, E., Rossi, V., Troupin, C., Faugère, Y., Pujol, I., & Pascual, A. (2014). Implications of refined altimetry on estimates of mesoscale activity and eddy-driven offshore transport in the Eastern Boundary Upwelling Systems. *Geophysical Research Letters*, *41*, 7602–7610. https://doi.org/10.1002/2014GL061770

Chaigneau, A., Dominguez, N., Eldin, G., Vasquez, L., Flores, R., Grados, C., & Echevin, V. (2013). Near-coastal circulation in the Northern Humboldt Current System from shipboard ADCP data. *Journal of Geophysical Research: Oceans*, *118*, 5251–5266. https://doi.org/10.1002/jgrc.20328

Chaigneau, A., Eldin, G., & Dewitte, B. (2009). Eddy activity in the four major upwelling systems from satellite altimetry (1992–2007). *Progress in Oceanography*, *83*(1-4), 117–123. https://doi.org/10.1016/j.pocean.2009.07.012

Chaigneau, A., Le Texier, M., Eldin, G., Grados, C., & Pizarro, O. (2011). Vertical structure of mesoscale eddies in the eastern South Pacific Ocean: A composite analysis from altimetry and Argo profiling floats. *Journal of Geophysical Research: Oceans*, *116*, C11025. https://doi.org/10.1029/2011JC007134

Chenillat, F., Franks, P. J. S., Rivière, P., Capet, X., Grima, N., & Blanke, B. (2015). Mesoscale activity in the Southern California Current System. Biological dynamics of a coastal eddy. *Journal of Geophysical Research: Oceans*, *120*, 5566–5588. https://doi.org/10.1002/2015JC010826

Contreras, M., Pizarro, O., Dewitte, B., Sepulveda, H. H., & Renault, L. (2019). Subsurface mesoscale eddy generation in the ocean off central Chile. *Journal of Geophysical Research*, *124*, 5700–5722. https://doi.org/10.1029/2018JC014723

Correa-Ramirez, M. A., Hormazabal, S., & Yuras, G. (2007). Mesoscale eddies and high chlorophyll concentrations off central Chile (29°–39°S). *Geophysical Research Letters*, *34*, L12604. https://doi.org/10.1029/2007GL029541

Correa-Ramirez, M. A., Rodriguez-Santana, A., Ricaurte-Villota, C., & Paramo, J. (2019). The Southern Caribbean upwelling system off Colombia: Water masses and mixing processes. *Deep Sea Research Part I: Oceanographic Research Papers*, *155*, 103145. https://doi.org/10.1016/j.dsr.2019.103145

Corredor-Acosta, A., Morales, C. E., Brewin, R. J. W., Auger, P. A., Pizarro, O., Hormazabal, S., & Anabalón, V. (2018). Phytoplankton size structure in association with mesoscale eddies off central-southern Chile: The satellite application of a phytoplankton size-class model. *Remote Sensing*, *10*(6), 834. https://doi.org/10.3390/rs10060834

Czeschel, R., Schütte, F., Weller, R. A., & Stramma, L. (2018). Transport, properties and life cycles of mesoscale eddies in the eastern tropical South Pacific. *Ocean Science*, *14*(4), 731–750. https://doi.org/10.5194/os-14-731-2018

D'Asaro, E., Lee, C., Rainville, L., Harcourt, R., & Thomas, L. (2011). Enhanced turbulence and energy dissipation at ocean fronts. *Science*, *332*(6027), 318–322. https://doi.org/10.1126/science.1201515

de Boyer Montégut, C., Madec, G., Fischer, A. S., Lazar, A., & Iudicone, D. (2004). Mixed layer depth over the global ocean: An examination of profile data and a profile-based climatology. *Journal of Geophysical Research*, *109*, C12003. https://doi.org/10.1029/2004JC002378

de Verneil, A., Franks, P. J. S., & Ohman, M. D. (2019). Frontogenesis and the creation of fine-scale vertical phytoplankton structure. *Journal of Geophysical Research: Oceans*, *124*, 1509–1523. https://doi.org/10.1029/2018JC014645

Dewar, W. K., McWilliams, J. C., & Molemaker, M. J. (2015). Centrifugal instability and mixing in the California undercurrent. *Journal of Physical Oceanography*, *45*(5), 1224–1241. https://doi.org/10.1175/JPO-D-13-0269.1

Dillon, T. M. (1982). Vertical overturns: A comparison of Thorpe and Ozmidov length scales. *Journal of Geophysical Research*, *87*(C12), 9601–9613. https://doi.org/10.1029/JC087iC12p09601

Doubell, M. J., Spencer, D., van Ruth, P. D., Lemckert, C., & Middleton, J. F. (2018). Observations of vertical turbulent nitrate flux during summer in the Great Australian Bight. *Deep Sea Research Part II: Topical Studies in Oceanography*, *157-158*, 27–35. https://doi.org/10.1016/j.dsr.2018.08.007

Ferron, B., Mercier, H., Speer, K., Gargett, A., & Polzin, K. (1998). Mixing in the Romanche Fracture Zone. *Journal of Physical Oceanography*, *28*(10), 1929–1945. https://doi.org/10.1175/1520-0485(1998)028<1929:MITRFZ>2.0.CO;2

Finkel, Z. V., Beardall, J., Flynn, K. J., Quigg, A., Rees, T. A. V., & Raven, J. A. (2010). Phytoplankton in a changing world: Cell size and elemental stoichiometry. *Journal of Plankton Research*, *32*(1), 119–137. https://doi.org/10.1093/plankt/fbp098

Franks, P. J. S., & Walstad, L. (1997). Phytoplankton patches at fronts: A model of formation and response to wind events. *Journal of Marine Research*, *55*(1), 1–29. https://doi.org/10.1357/0022240973224472

Frants, M., Damerell, G. M., Gille, S. T., Heywood, K. J., MacKinnon, J., & Sprintall, J. (2013). An assessment of density-based finescale methods for estimating diapycnal diffusivity in the Southern Ocean. *Journal of Atmospheric and Oceanic Technology*, *30*(11), 2647–2661. https://doi.org/10.1175/JTECH-D-12-00241.1

Gargett, A., & Garner, T. (2008). Determining Thorpe scales from ship-lowered CTD density profiles. *Journal of Atmospheric and Oceanic Technology*, *25*(9), 1657–1670. https://doi.org/10.1175/2008JTECHO541.1

Girault, M., Arakawa, H., Barani, A., Ceccaldi, H. J., Hashihama, F., & Gregori, G. (2015). Heterotrophic prokaryote distribution along a 2300 km transect in the North Pacific subtropical gyre during a strong La Niña conditions: Relationship between distribution and hydrological conditions. *Biogeosciences*, *12*(11), 3607–3621. https://doi.org/10.5194/bg-12-3607-2015

Hales, B., Hebert, D., & Marra, J. (2009). Turbulent supply of nutrients to phytoplankton at the New England shelf break front. *Journal of Geophysical Research*, *114*, C05010. https://doi.org/10.1029/2008JC005011

Hales, B., Moum, J. N., Covert, P., & Perlin, A. (2005). Irreversible nitrate fluxes due to turbulent mixing in a coastal upwelling system. *Journal of Geophysical Research*, *110*, C10S11. https://doi.org/10.1029/2004JC002685

Harrison, C. S., & Siegel, D. A. (2014). The tattered curtain hypothesis revised: Coastal jets limit cross-shelf larval transport. *Limnology and Oceanography: Fluids and Environments.*, *4*(1), 50–66. https://doi.org/10.1215/21573689-2689820

Henley, S. F., Jones, E. M., Venables, H. J., Meredith, M. P., Firing, Y. L., Dittrich, R., et al. (2018). Macronutrient and carbon supply, uptake and cycling across the Antarctic Peninsula shelf during summer. *Philosophical Transactions of the Royal Society A - Mathematical Physical and Engineering Sciences*, *376*(2122), 20170168. https://doi.org/10.1098/rsta.2017.0168

Hormazabal, S., Combes, V., Morales, C. E., Correa-Ramirez, M. A., Di Lorenzo, E., & Nuñez, S. (2013). Intrathermocline eddies in the coastal transition zone off central Chile (31–41°S). *Journal of Geophysical Research*, *118*, 4811–4821. https://doi.org/10.1002/jgrc.20337

Hsu, P. C., Cheng, K. H., Jan, S., Lee, H. J., & Ho, C. R. (2019). Vertical structure and surface patterns of Green Island wakes induced by the Kuroshio. *Deep Sea Research Part I: Oceanographic Research Papers*, *143*, 1–16. https://doi.org/10.1016/j.dsr.2018.11.002

Johnson, G. C., & McTaggart, K. E. (2010). Equatorial Pacific 13°C water eddies in the eastern subtropical South Pacific Ocean. *Journal of Physical Oceanography*, *40*(1), 226–236. https://doi.org/10.1175/2009JPO4287.1

Johnston, T. M. S., Rudnick, D. L., & Pallàs-Sanz, E. (2011). Elevated mixing at a front. *Journal of Geophysical Research*, *116*, C11033. https://doi.org/10.1029/2011JC007192

Klein, P., & Lapeyre, G. (2009). The oceanic vertical pump induced by mesoscale and submesoscale turbulence. *Annual Review of Marine Science*, *1*(1), 351–375. https://doi.org/10.1146/annurev.marine.010908.163704

Klein, P., Lapeyre, G., Siegelman, L., Qiu, B., Fu, L.-L., Torres, H., et al. (2019). Ocean-scale interactions from space. *Earth and Space Science.*, *6*, 795–817. https://doi.org/10.1029/2018ea000492 2018EA000492

Klymak, J. M., Pinkel, R., & Rainville, L. (2008). Direct breaking of the internal tide near topography: Kaena Ridge, Hawaii. *Journal of Physical Oceanography*, *38*(2), 380–399. https://doi.org/10.1175/2007JPO3728.1

Krause, J. W., Brzezinski, M. A., Goericke, R., Landry, M. R., Ohman, M. D., Stukel, M. R., & Taylor, A. G. (2015). Variability in diatom contributions to biomass, organic matter production and export across a frontal gradient in the California Current Ecosystem. *Journal of Geophysical Research: Oceans*, *120*, 1032–1047. https://doi.org/10.1002/2014JC010472

Lamont, T., Barlow, R. G., & Brewin, R. J. W. (2018). Variations in remotely-sensed phytoplankton size structure of a cyclonic eddy in the Southwest Indian Ocean. *Remote Sensing*, *10*(7), 1143. https://doi.org/10.3390/rs10071143

Law, C. S., Martin, A. P., Liddicoat, M. I., Watson, A. J., Richards, K. J., & Woodward, E. M. S. (2001). A Lagrangian SF6 tracer study of an anticyclonic eddy in the North Atlantic: Patch evolution, vertical mixing and nutrient supply to the mixed layer. *Deep Sea Research Part II: Topical Studies in Oceanography.*, *48*(4-5), 705–724. https://doi.org/10.1016/S0967-0645(00)00112-0

Ledwell, J. R., McGillicuddy, D. J. Jr., & Anderson, L. A. (2008). Nutrient flux into an intense deep chlorophyll layer in a mode-water eddy. *Deep Sea Research Part II: Topical Studies in Oceanography.*, *55*(10-13), 1139–1160. https://doi.org/10.1016/j.dsr2.2008.02.005

Letelier, J., Pizarro, O., & Nuñez, S. (2009). Seasonal variability of coastal upwelling and the upwelling front off central Chile. *Journal of Geophysical Research*, *114*, C12009. https://doi.org/10.1029/2008JC005171

Lévy, M., Franks, P. J., & Smith, K. S. (2018). The role of submesoscale currents in structuring marine ecosystems. *Nature Communications*, *9*(1), 4758. https://doi.org/10.1038/s41467-018-07059-3

Li, Q. P., Franks, P. J., Ohman, M. D., & Landry, M. R. (2012). Enhanced nitrate fluxes and biological processes at a frontal zone in the Southern California Current System. *Journal of Plankton Research*, *34*(9), 790–801. https://doi.org/10.1093/plankt/fbs006

Llanillo, P. J., Pelegrí, J. L., Duarte, C. M., Emelianov, M., Gasser, M., Gourrion, J., & Rodríguez-Santana, A. (2012). Meridional and zonal changes in water properties along the continental slope off central and northern Chile. *Ciencias Marinas*, *38*(1B), 307–332. https://doi.org/10.7773/cm.v38i1B.1814

Loginova, A. N., Thomsen, S., Dengler, M., Lüdke, J., & Engel, A. (2019). Diapycnal dissolved organic matter supply into the upper Peruvian oxycline. *Biogeosciences*, *16*(9), 2033–2047. https://doi.org/10.5194/bg-16-2033-2019

Lund-Hansen, L. C., Ayala, P. C. D. A., & Reglero, A. F. (2006). Bio-optical properties and development of a sub-surface chlorophyll maxima (SCM) in southwest Kattegat, Baltic Sea. *Estuarine, Coastal and Shelf Science*, *68*(1-2), 372–378. https://doi.org/10.1016/j.ecss.2006.02.019

Mahadevan, A. (2016). The impact of submesoscale physics on primary productivity of plankton. *Annual Review of Marine Science*, *8*(1), 161–184. https://doi.org/10.1146/annurev-marine-010814-015912

Mahadevan, A., & Tandon, A. (2006). An analysis of mechanisms for submesoscale vertical motion at ocean fronts. *Ocean Modelling*, *14*(3-4), 241–256. https://doi.org/10.1016/j.ocemod.2006.05.006

Marañón, E. (2015). Cell size as a key determinant of phytoplankton metabolism and community structure. *Annual Review of Marine Science*, *7*(1), 241–264. https://doi.org/10.1146/annurev-marine-010814-015955

Mater, B. D., Venayagamoorthy, S. K., St. Laurent, L., & Moum, J. N. (2015). Biases in Thorpe-scale estimates of turbulence dissipation. Part I: Assessments from large-scale overturns in oceanographic data. *Journal of Physical Oceanography*, *45*(10), 2497–2521. https://doi.org/10.1175/JPO-D-14-0128.1

McDougall, T. J., & P. M. Barker. (2011). Getting started with TEOS-10 and the Gibbs Seawater (GSW) Oceanographic Toolbox, 28pp. SCOR/IAPSO WG127, ISBN 978-0-646-55621-5.

McGillicuddy, D. J. Jr. (2016). Mechanisms of physical-biological-biogeochemical interaction at the oceanic mesoscale. *Annual Review of Marine Science*, *8*(1), 125–159. https://doi.org/10.1146/annurev-marine-010814-015606

Menschel, E., Gonzalez, H. E., & Giesecke, R. (2016). Coastal-oceanic distribution gradient of coccolithophores and their role in the carbonate flux of the upwelling system off Concepción, Chile (36°S). *Journal of Plankton Research*, *38*(4), 798–817. https://doi.org/10.1093/plankt/fbw037

Morales, C. E., Anabalón, V., Bento, J. P., Hormazabal, S., Cornejo, M., Correa-Ramírez, M. A., & Silva, N. (2017). Front-eddy influence on water column properties, phytoplankton community structure, and cross-shelf exchange of diatom taxa in the shelf-slope area off Concepción (~36–37°S). *Journal of Geophysical Research: Oceans*, *122*, 8944–8965. https://doi.org/10.1002/2017JC013111

Morales, C. E., Hormazabal, S., Correa-Ramírez, M., Pizarro, O., Silva, N., Fernandez, C., et al. (2012). Mesoscale variability and nutrient-phytoplankton distributions off central-southern Chile during the upwelling season: The influence of mesoscale eddies. *Progress in Oceanography*, *104*, 17–29. https://doi.org/10.1016/j.pocean.2012.04.015

Mouw, C. B., Barnett, A., McKinley, G. A., Gloege, L., & Pilcher, D. (2016). Phytoplankton size impact on export flux in the global ocean. *Global Biogeochemical Cycles*, *30*(10), 1542–1562. https://doi.org/10.1002/2015GB005355

Nagai, T., Gruber, N., Frenzel, H., Lachkar, Z., McWilliams, J. C., & Plattner, G.-K. (2015). Dominant role of eddies and filaments in the offshore transport of carbon and nutrients in the California Current System. *Journal of Geophysical Research: Oceans*, *120*, 5318–5341. https://doi.org/10.1002/2015JC010889

Omand, M. M., D'Asaro, E. A., Lee, C. M., Perry, M. J., Briggs, N., Cetinić, I., & Mahadevan, A. (2015). Eddy-driven subduction exports particulate organic carbon from the spring bloom. *Science*, *348*(6231), 222–225. https://doi.org/10.1126/science.1260062

Osborn, T. R. (1980). Estimates of the local rate of vertical diffusion from dissipation measurements. *Journal of Physical Oceanography*, *10*(1), 83–89. https://doi.org/10.1175/1520-0485(1980)010<0083:EOTLRO>2.0.CO;2

Ozmidov, R. V. (1965). On the turbulent exchange in a stably stratified ocean. *Izv. Acad. Sci. USSR. Atmos. Oceanic Phys.*, *1*, 861–871.

Park, Y. H., Lee, J. H., Durand, I., & Hong, C. S. (2014). Validation of Thorpe-scale-derived vertical diffusivities against microstructure measurements in the Kerguelen region. *Biogeosciences*, *11*(23), 6927–6937. https://hal.sorbonne-universite.fr/hal-01308076. https://doi.org/10.5194/bg-11-6927-2014

Pegliasco, C., Chaigneau, A., & Morrow, R. (2015). Main eddy vertical structures observed in the four major Eastern Boundary Upwelling Systems. *Journal of Geophysical Research: Oceans*, *120*, 6008–6033. https://doi.org/10.1002/2015JC010950

Pérez-Santos, I., Garcés-Vargas, J., Schneider, W., Ross, L., Parra, S., & Valle-Levinson, A. (2014). Double-diffusive layering and mixing in Patagonian fjords. *Progress in Oceanography*, *129*, 35–49. https://doi.org/10.1016/j.pocean.2014.03.012

Pietri, A., Testor, P., Echevin, V., Chaigneau, A., Mortier, L., Eldin, G., & Grados, C. (2013). Finescale vertical structure of the upwelling system off southern Peru as observed from glider data. *Journal of Physical Oceanography*, *43*(3), 631–646. https://doi.org/10.1175/JPO-D-12-035.1

Pond, S., & Pickard, G. L. (2013). *Introductory dynamical oceanography* (2nd ed.). Oxford: Elsevier.

Richardson, T. L. (2019). Mechanisms and pathways of small-phytoplankton export from the surface ocean. *Annual Reviews in Marine Science.*, *11*(1), 57–74. https://doi.org/10.1146/annurev-marine-121916-063627

Rippeth, T. P., Wiles, P., Palmer, M. R., Sharples, J., & Tweddle, J. (2009). The diapcynal nutrient flux and shear-induced diapcynal mixing in the seasonally stratified western Irish Sea. *Continental Shelf Research*, *29*(13), 1580–1587. https://doi.org/10.1016/j.csr.2009.04.009

Rodríguez, J., Tintoré, J., Allen, J. T., Blanco, J. M., Gomis, D., Reul, A., & Jiménez-Gómez, F. (2001). Mesoscale vertical motion and the size structure of phytoplankton in the ocean. *Nature*, *410*(6826), 360–363. https://doi.org/10.1038/35066560

Sangrà, P., García-Muñoz, C., García, C. M., Marrero-Díaz, A., Sobrino, C., & Mouriño-Carballido, B. (2014). Coupling between upper ocean layer variability and size-fractionated phytoplankton in a non-nutrient-limited environment. *Marine Ecology Progress Series*, *499*, 35–46. https://doi.org/10.3354/meps10668

Scotti, A. (2015). Biases in Thorpe-scale estimates of turbulence dissipation. Part II: energetics arguments and turbulence simulations. *Journal of Physical Oceanography*, *45*(10), 2522–2543. https://doi.org/10.1175/JPO-D-14-0092.1

Silva, N., Rojas, N., & Fedele, A. (2009). Water masses in the Humboldt Current System: Properties, distribution, and the nitrate deficit as a chemical water mass tracer for Equatorial Subsurface Water off Chile. *Deep Sea Research Part II: Topical Studies in Oceanography.*, *56*(16), 1004–1020. https://doi.org/10.1016/j.dsr2.2008.12.013

Steinfeldt, R., Sültenfuß, J., Dengler, M., Fischer, T., & Rhein, M. (2015). Coastal upwelling off Peru and Mauritania inferred from helium isotope disequilibrium. *Biogeosciences*, *12*(24), 7519–7533. https://doi.org/10.5194/bg-12-7519-2015

Stramma, L., Bange, H. W., Czeschel, R., Lorenzo, A., & Frank, M. (2013). On the role of mesoscale eddies for the biological productivity and biogeochemistry in the eastern tropical Pacific Ocean off Peru. *Biogeosciences*, *10*(11), 7293–7306. https://doi.org/10.5194/bg-10-7293-2013

Strub, P. T., Mesias, J. M., Montecino, V., Rutllant, J., & Salinas, S. (1998). Coastal ocean circulation off western South America. In A. Robinson, & K. Brink (Eds.), *The sea* (Vol. 11, pp. 273–313). New York, NY: John Wiley.

Taylor, A. G., Goericke, R., Landry, M. R., Selph, K. E., Wick, D. A., & Roadman, M. J. (2012). Sharp gradients in phytoplankton community structure across a frontal zone in the California Current Ecosystem. *Journal of Plankton Research*, *34*(9), 778–789. https://doi.org/10.1093/plankt/fbs036

Thomas, L. N., & Taylor, J. R. (2010). Reduction of the usable wind-work on the general circulation by forced symmetric instability. *Geophysical Research Letters*, *37*, L18606. https://doi.org/10.1029/2010GL044680

Thomsen, S., Kanzow, T., Krahmann, G., Greatbatch, R. J., Dengler, M., & Lavik, G. (2016). The formation of a subsurface anticyclonic eddy in the Peru-Chile Undercurrent and its impact on the near-coastal salinity, oxygen, and nutrient distributions. *Journal of Geophysical Research: Oceans*, *121*, 476–501. https://doi.org/10.1002/2015JC010878

Thyng, K. M., Greene, C. A., Hetland, R. D., Zimmerle, H. M., & DiMarco, S. F. (2016). True colors of oceanography: Guidelines for effective and accurate colormap selection. *Oceanography* https://doi.org/10.5670/, *29*(3), 9–13.

Vergara, O. A., Echevin, V., Sepulveda, H. H., Colas, F., & Quiñones, R. A. (2016). Modelling the seasonal dynamics of the Peru-Chile Undercurrent off central Chile (30–40°S). *Continental Shelf Research*, *123*, 61–79. https://doi.org/10.1016/j.csr.2016.04.001

Waga, H., Hirawake, T., & Ueno, H. (2019). Impacts of mesoscale eddies on phytoplankton size structure. *Geophysical Research Letters*, *46*, 13,191–13,198. https://doi.org/10.1029/2019GL085150

Zhang, J. Z., Baringer, M. O., & Fischer, C. J. (2017). An estimate of diapcynal nutrient fluxes to the euphotic zone in the Florida Straits. *Scientific Reports*, *7*(1), 16098. https://doi.org/10.1038/s41598-017-15853-0

Zhang, S., Curchitser, E. N., Kang, D., Stock, C. A., & Dussin, R. (2018). Impacts of mesoscale eddies on the vertical nitrate flux in the Gulf Stream region. *Journal of Geophysical Research: Oceans*, *123*, 497–513. https://doi.org/10.1002/2017JC013402